# Mapping age and basal conditions of ice in the Dome Fuji region, Antarctica, by combining radar internal layer stratigraphy and flow modeling

Zhuo Wang[1,2], Ailsa Chung[3], Daniel Steinhage[1], Frédéric Parrenin[3], Johannes Freitag[3], and Olaf Eisen[1,4]

[1]Alfred-Wegener-Institut, Helmholtz-Zentrum für Polar und Meeresforschung, Bremerhaven, Germany
[2]College of Geo-Exploration and Technology, Jilin University, Changchun, China
[3]Univ. Grenoble Alpes, CNRS, IRD, IGE, Grenoble, France
[4]Department of Geosciences, Universität Bremen, Bremen, Germany

**Correspondence:** Olaf Eisen (olaf.eisen@awi.de)

**Abstract.** The Dome Fuji (DF) region in Antarctica is a potential site for an ice core with a record of over one million years. Here, we combine ~~the~~ large-scale internal airborne radar stratigraphy with a 1-D model to estimate the age of basal ice in the DF region. The radar data used in the study were collected in a survey during the 2016–2017 Antarctica season. We transfer the newest age–depth scales from the DF ice core to isochrones ~~in~~ traced in radargrams in the surrounding 500 km × 550 km region~~through traced radar isochrones~~. At each point of the survey the 1-D model uses the ages of isochrones to construct the age–depth scale at depths where dated isochrones do not exist, the ~~basal thermal conditions, including~~ surface accumulation rate and the basal thermal condition, including melt rate and the thickness of ~~a potentially present basal layer and surface accumulation rates~~stagnant ice. Our resulting age distribution and age density suggest that ~~a few~~ several promising sites with ice older than 1.5 million years in the DF region might exist. The deduced melt rates and presence of stagnant ice ~~map provides~~ provide more constraints for ~~finding~~ locating sites with a cold base. The accumulation rates range from 0.015 to 0.038 m $a^{-1}$ ice equivalent. ~~The~~ Based on sensitivity studies we find that the numbers of picked isochrones and the timescale of the ice core severely affect the model results~~according to sensitivity studies~~. Our study demonstrates ~~it is possible to find the old ice in the DF region, and the constraint~~ that constraints from deep radar isochrones and a trustworthy timescale could improve the model estimation to find old ice in the DF region.

## 1 Introduction

~~To~~ In order to understand the Quaternary climate, the progression of glaciations and the carbon cycle, we need to find continuous and undisturbed ice-core records back to 1.5 million years BP (before present, present defined as 1950) ~~are crucial~~ (Fischer et al., 2013; Jouzel and Masson-Delmotte, 2010). The ~~mid-Pleistocene transition (MPT), which occurred in the time interval between 1200 ka and 900 ka BP, termed by a~~ switch from more regular 41 ka glacial ~~cycle~~ cycles (1500 to 1200 ka BP) to current 100 ka glacial ~~cycle (Lisiecki and Raymo, 2005), is~~ cycles, which occurred in the time interval between 1200 ka and 900 ka BP, is known as the mid-Pleistocene transition (MPT) and is still not fully understood (Lisiecki and Raymo, 2005). $CO_2$ and other greenhouse gas may have either forced this switch or might have responded to it (Willeit et al., 2019). A direct record

of greenhouse gases with atmospheric record covering this period can only be found in Antarctica ice ~~core~~ cores (Fischer et al., 2013). Moreover, isotopic and chemical records in ice cores of that age can provide additional information on temperature, ice dynamic changes and magnetic reversals, ~~to~~ which can be analyzed together with other marine and terrestrial records (Raymo et al., 2006; Raisbeck et al., 2006; Singer and Brown, 2002). Hence, identifying "Oldest Ice" sites in Antarctica is one of the primary challenges for ice-core research.

~~There~~ It is a huge challenge ~~in retrieving continuous records of old ice cores where~~ to retrieve continuous old ice-core records, as the oldest ice is compressed in deep layers near the base of the ice sheet. Ice older than one million years could have melted away by reaching the pressure melting point or be disturbed, and thus not ~~feasible~~ useful for ice-core analyses, because of complicated processes in the ~~basal layer~~ deepest ice (Van Liefferinge and Pattyn, 2013). As one consortium in the International Partnerships in Ice Core Sciences (IPICS), the European "Beyond EPICA–Oldest Ice" (BE–OI) consortium initiated pre-site surveys in the wider Dome Concordia (DC) and Dome Fuji (DF) regions. ~~Van Liefferinge and Pattyn (2013)~~ Van Liefferinge and Pattyn (2013) evaluated potential sites of million year-old ice in Antarctica considering ice velocity, ice thickness and geothermal heat flow (GHF) based on a ~~thermo-dynamical~~ thermodynamical model. In a follow-up study, ~~Van Liefferinge et al. (2018)~~ Van Liefferinge et al. (2018) focused on more detailed sites for oldest ice in the DF and DC regions~~leveraging~~ , using more robust criteria ~~of~~ (for ice thickness and velocity~~, and using~~ ), and a metric for the shape of the bed. In the DC region, ~~Young et al. (2017) proposed some old ice targets~~ Young et al. (2017) extended ice thickness coverage, mapped the basal roughness and found more subglacial lakes through high-resolution aerogeophysical surveys, and ~~Parrenin et al. (2017)~~ finally assessed the previous old ice candidates. Parrenin et al. (2017) inferred the age of ice ~~and further~~ based on 1-D thermo-mechanical model constrained by radar observations and identified two target areas where ice older than 1.5 Ma may exist~~, based on 1-D thermo-mechanical model constrained by radar observations. Lilien et al. (2021)~~ . Lilien et al. (2021) refined the age–depth scale at Little Dome C (LDC), 40 km from the DC site, ~~based on a~~ by adapting a 1-D ice flow model constrained by high-resolution radar ~~survey on the drilling site determined~~ data collected around the drill site selected for the Beyond EPICA project. They suggested 1.5 Myr old ice exists at $\sim$ 2500 m depth, where stratigraphy is still intact and preserved with analysable resolution. In the Dome A region, ~~Sun et al. (2014)~~ Sun et al. (2014) estimated ice age around Kunlun station by applying a three-dimensional, thermomechanically coupled full-Stokes model, which indicated that in the area without basal melting the ice age at 95 % depth could be limited to 1.5 Ma. Beem et al. (2021) suggested that Titan Dome is an unlikely to have old ice covering MPT based on depth distribution of dated internal horizons traced in the radar data, age modeling constrained by radar horizons and faster flow that ceased during the last glacial maximum.

The Dome Fuji region is a potential area for holding oldest ice in Antarctica. The DF ~~station and site of two previous ice-core drillings, is located at~~ drill site (77°19′01″ S, 39°42′12″ E~~(Ageta et al., 1998)~~ ) (Ageta et al., 1998) is located at an elevation of 3810 m, with an ice thickness of 3028±15 m (Fujita et al., 1999, 2015), an annual mean air temperature of −54.4°C (Kameda et al., 2009) and ~~an~~ a mean annual accumulation of $\sim$ 24 mm w.e.a$^{-1}$ (Fujita et al., 2011). The first deep ice core at DF, which was drilled from 1995 to 1996, reached 2503.52 m and covered ~~a record back to~~ the past $\sim$ 340 ka ~~dated by~~ using the isotopic $\delta^{18}$O record ~~(Ageta et al., 1998; Watanabe et al., 1999). Kawamura et al. (2007)~~ for dating (Ageta et al., 1998; Watanabe et al., 1999). Kawamura et al. (2007) used $O_2/N_2$ measurements, a proxy of local sum-

mer insolation, to build a new timescale (referred to as DFO-2006). Based on these $O_2/N_2$ age markers, ~~Parrenin et al. (2007)~~ Parrenin et al. (2007) used a 1-D ice flow model to reconstruct the timescale down to ~~basal ice~~ the ice near the base and accumulation rates (referred to as DFGT-2006). During the austral summers from 2003/04 to 2006/07, the second deep ice core, only 48 m away from the first ~~ice core~~ one (Saruya et al., 2022), was finally drilled to a depth of 3035.22 m. It is considered to be very closed to the bedrock (Motoyama, 2007; Motoyama et al., 2021) and the temperature at the bottom of this ~~ice core~~ borehole reached the melting point (Talalay et al., 2020). ~~The Dome Fuji Ice Core Project Members (2017) dated this deep ice core back to ~ 720 ka by~~ By synchronising the isotopic $\delta^{18}O$ record of the DF ice core with that of the ice core at DC (AICC2012)~~and accumulation rates were also deduced from the $\delta^{18}O$ record~~, Dome Fuji Ice Core Project Members (2017) dated the DF deep ice core back to ~ 720 ka and deduced accumulation rates. A timescale which combines DFO-2006 (< 342 ka) and AICC2012 (> 344 ka) was ~~proposed then~~ then proposed (referred to as DFO2006+AICC2012) ~~.~~ (Dome Fuji Ice Core Project Members, 2017) .

In addition to the direct analysis of ice-core proxies, ~~Seddik et al. (2011) simulated the temperature at the ice base and the age at 95 % of the depth with the Continuum-mechanical Anisotropic Flow model in~~ some ice models were applied in the larger DF region to investigate basal thermal states and age fields. Seddik et al. (2011) adapted a three-dimensional, thermomechanically coupled ice flow model with induced anisotropy to a ~ 200 km × 200 km domain around the DF drill site. ~~Karlsson et al. (2018)~~ They simulated a basal melt rate of ~ 0.35 mm $a^{-1}$ at DF, and found that the consideration of anisotropy would decrease the inferred age of the ice. Karlsson et al. (2018) presented an updated subglacial topography with a resolution of 10 km in the DF region based on ~~an~~ airborne radar surveys conducted by the Alfred Wegener Institute, Helmholtz Centre for Polar and Marine Research (AWI), as part of the Beyond EPICA project. ~~They~~ With new bed topography, they refined some promising oldest ice sites proposed by ~~Van Liefferinge and Pattyn (2013)~~ Van Liefferinge and Pattyn (2013) using the same model ~~. Their updated age estimates suggested three main areas with potential oldest ice candidates in the DF region. Tsutaki et al. (2022)~~ and suggested that especially the region immediately south of Dome Fuji station is promising for holding old ice. A 1-D ice flow model called IcIES-2 was adapted to DF and the DF-New Dome Fuji site (NDF) transect by Obase et al. (2023). They examined the influence of ice thickness and GHF on the age of the ice and pointed out that ice thickness is one of the most critical factors for the preservation of old ice. They suggested that analyzable 1.5 Ma old ice could be expected at DF when the GHF is small enough to keep the basal ice from melting.

Tsutaki et al. (2022) compiled a new ice thickness ~~dataset with a resolution of 0.5 km based on~~ data set collected by ground-based ~~radar measurements collected by Japanese Antarctic Research Expedition (JARE), to examine~~ radar surveys over the last 30 years, which revealed higher resolution of the complex landscapes compared with the previous data sets. Based on the new compilation, they examined roughness and slope of the ice–bed interface, the stress state of the ice and the subglacial hydrological conditions in the vicinity of DF and ~~the so-called New Dome Fuji site (NDF), which focused on a smaller region for old ice. ? simulated temperature, basal melt rates and age profiles through a 1-D ice flow model, IcIES-2, along the DF-NDF transect.~~ NDF, thus provided a substantial set of constraints for identifying old ice candidate sites.

~~Despite of all these progresses, age estimates and~~ We present another method to complement the progress already made by constraining age and the basal thermal condition in the larger DF region (i.e. roughly a 500 km × 550 km perimeter) ~~are not~~

~~yet constrained~~ by isochrones detected by radar. ~~Here, we~~ We connect the ice-internal isochrone stratigraphy in the larger DF region to the DF drill site through isochrones traced in the airborne radar data collected during the 2016–17 survey conducted by AWI. We apply a 1-D ice flow model (see more details of the model in the companion paper of ~~Chung et al. (2023)) to model~~ Chung et al. (2023)) to determine the age–depth scale below the available isochrone stratigraphy, accumulation rates and also to derive either melt rates or the thickness of ~~a (potentially stagnant ) basal layer of~~ the stagnant ice in the DF region. We finally discuss the reliability of the results, conduct sensitivity experiments to quantify the effect of ~~picked isochrones numbers~~ the number of used isochrone and the timescale of the ice core on our age estimates as well as the other modeling results.

## 2 Data and Methods

### 2.1 Data collection

We ~~use data collected with the~~ acquired 26 radar profiles with the AWI airborne radio-echo sounding (RES) system ~~of the AWI mounted on its~~ operated on the Basler BT-67 aircraft Polar6 (Wesche et al., 2016) during the 2016/17 Antarctic season. The radar survey was conducted ~~in the DF region,~~ from a temporary camp (79° S, 30° E) 290 km ~~away~~ south-west from the DF station~~, where 26 radar profiles were recorded~~. Survey lines have parallel line spacing of 10 km in the northern part of the study area and 15 km line spacing in the southern part ~~, the spacing distance is getting much smaller~~ with smaller spacing distances when approaching and leaving the camp (Karlsson et al., 2018). ~~In our study we include~~ Of the 26 profiles available we analyse 22 ~~survey profiles~~ with lengths varying from 622 km to 898 km. The study area covers a region of about 270,000 km$^2$ and an elevation range of about 3400 m–3810 m (Fig. 1). In this region, ice surface velocities range from 0 to 5.8 m a$^{-1}$.

The AWI RES system transmits radar waves with a center frequency of 150 MHz, a band width of 20 MHz and an amplitude of 1.6 kW. During the survey it ~~only operated~~ effectively operated as a pulse-limited radar with the 600 ns ~~long pulse, thus effectively operating as a pulse-limited radar~~wide pulse. The theoretical vertical resolution in ice for the 600 ns burst is 50 m (Nixdorf et al., 1999). In this study we use radar returns of the 600 ns long burst from internal reflection horizons (IRHs) as well as from the ice–bedrock interface. The raw radar data has a mean spacing of 5 m along the flight line (which varies with real speed and direction of aircraft) and is sampled at ~~an~~ a time interval of 4 ns (Karlsson et al., 2018).

Before picking the IRHs and the ice–bed interface, the radar data are resampled to 12 ns and stacked 7 fold, which ~~lead~~ leads to a mean trace spacing of $\sim$ 35 m. In addition, a low-pass filter and a ~~two-dimension~~ running average filter are used to decrease noise. Automatic gain control (AGC) is used to balance the gain and facilitate ~~layer~~ horizon tracing. Processing is performed in the seismic environment of the Echos software from Paradigm Geophysical.

### 2.2 ~~Horizons~~ Horizon picking and dating

In order to provide age markers (i.e., the age of IRHs) and ice thickness to use as ~~observations~~ constraints in our 1-D flow model, IRHs are traced in the two-way travel time (TWT) domain. The surface reflection is picked automatically in ~~Echos~~ the program "Echos" and then subtracted in all traces to shift the first break of the radar data to time zero. The maximum reflection

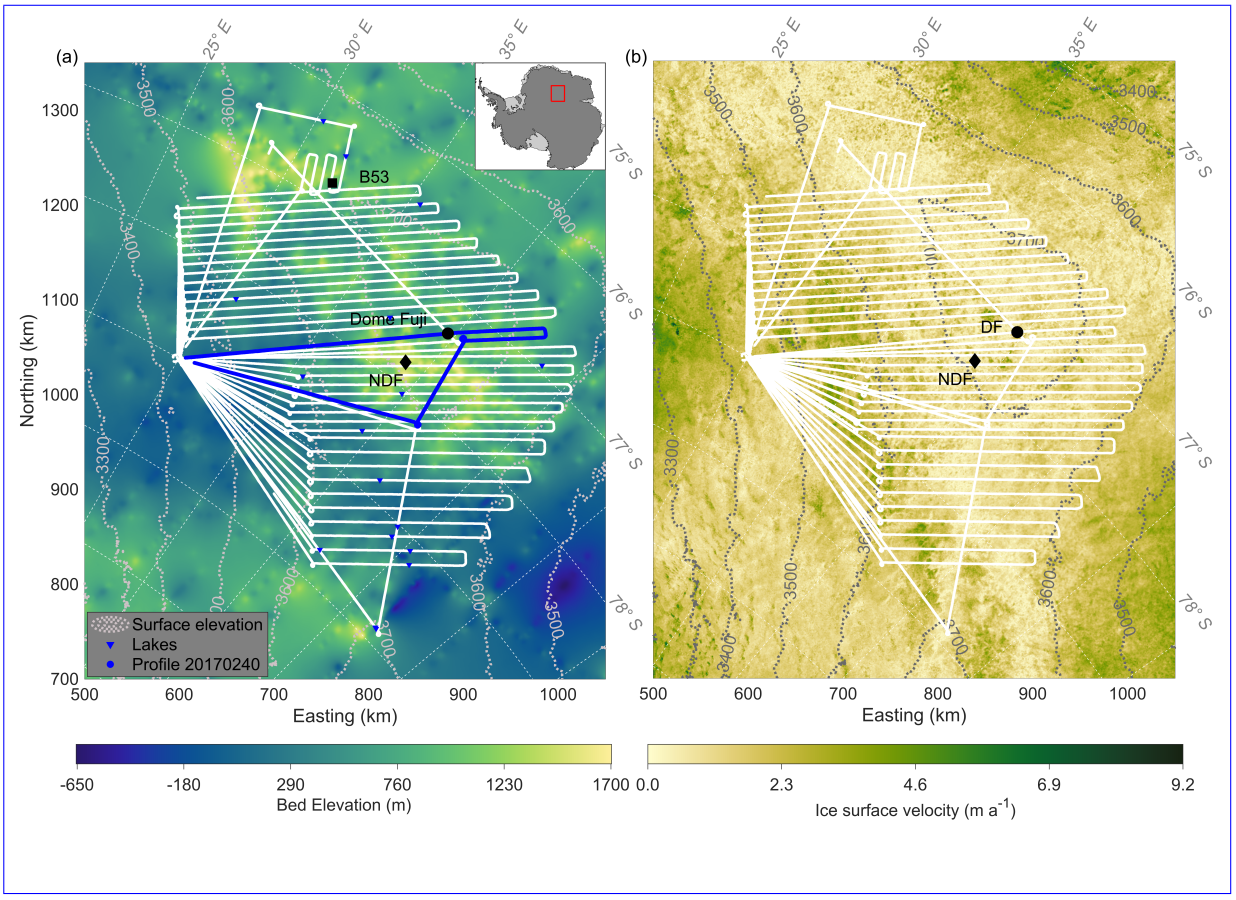


**Figure 1.** (a) Study area in the DF region, with inset showing the position in Antarctica. The white lines represent the radar survey profiles used in our study. The blue line shows the ~~exemplary~~ example profile 20170240. We use surface elevation (contour map) and bed elevation from ~~Greene et al. (2017)~~ Morlighem et al. (2020) and ~~Morlighem et al. (2017, 2020)~~Morlighem (2022). Subglacial lakes were identified by ~~Karlsson et al. (2018)~~Karlsson et al. (2018). (b) Ice surface velocities mapped by (Rignot et al., 2017, 2011; Mouginot et al., 2012, 2017).

power of IRHs is traced manually in the seismic software package ~~Section~~"Section", which allows IRHs to be continuously traced in different radar profiles through intersections between profiles. This ensures that the same isochronous horizons are traced. We trace 6 (H1, H2, H4–H7) or 7 (H1–H7) relatively distinct and continuous IRHs ~~(H1–H7) in all survey lines,~~ in the radar profiles, since the third IRH H3 is not clear and continuous enough to be traced in some profiles. Ice–bed returns were picked by ~~Karlsson et al. (2018)~~ Karlsson et al. (2018) through semi-automatic detection routines in ~~Matlab.~~ MATLAB. These ice thickness data are available on PANGAEA (Eisen et al., 2020). The ice–bed returns are often diffuse~~events~~, especially around mountain peaks, which results in disagreements when using different methods to trace ice–bed returns, and thus differences in ice thickness and modeling results. We emphasize that ~~Karlsson et al. (2018)~~ Karlsson et al. (2018) picked the

first (uppermost) ice–bed return when there were uncertainties, so that ice thickness estimates can be considered a minimum ice thickness in some places.

TWT is converted to depth assuming a constant radar wave speed of 168.5 m $\mu s^{-1}$ in ice (Winter et al., 2017; Lilien et al., 2021) and a 15.5 m firn correction calculated from depth-density curve in the B53 ice core. The B53 ice core was drilled to 202 m depth by the AWI team ~~,~~ during the survey period and is located at 79°47′38″ S, 31°54′19″ E, and ∼ 203.5 km away from the DF drill site (Fig. 1). The point of closest approach to the DF drill site on our radar profiles is located ∼ 91.1 m away~~from the DF drill site~~, at 77°19′ S, 39°41′59″ E, on the profile 20170240. Ice thickness at this ~~closest point observed from~~ nearest point observed in the radargram is about 3044.8 m, and the ice thickness ~~in~~ at the DF drill site interpolated ~~from~~ between our radar observations is about 3050.5 m. This corresponds within the the uncertainty estimates with a previously inferred ice thickness of 3028±15 m from a radar observation (Fujita et al., 1999), and it approximates the depth of the second DF deep ice core, 3035.2 m, which is considered to be very close to ice–bed interface (Motoyama, 2007).

IRHs at this location closest to the DF drill site are firstly converted to depth and then dated by vertical interpolation of the ages from the DFO2006+AICC2012 timescale (Dome Fuji Ice Core Project Members, 2017), available to a depth of 3031 m with an ice age of 715.9 ka BP, and ~~then~~ finally transferred to the radargram at the depths of the IRHs. Fig. 2 shows traced IRHs H1–H7 in the profile 20170240 with the point of closest approach shown as white vertical line. The age of IRHs, ranging from 31.4 ka (H1) to 169.1 ka (H7), and their age uncertainty, are marked in Fig. 2. Ages of different IRHs are then transferred to all profiles via our network, which then serve as the primary ~~input~~ constraint to the 1-D model.

### 2.3 Age uncertainty of internal reflection horizons

The uncertainty of IRH age estimates directly ~~impact~~ impacts the reliability of the results from the model, as it includes uncertainty of the ice-core agescale and age uncertainty caused by depth uncertainty of IRHs. ~~As for~~ For the depth uncertainty of IRHs, we consider slope-induced ~~uncertainty~~ uncertainties caused by the offset of the closest radargram to the DF drill site, ~~uncertainty of~~ of the firn correction, ~~uncertainty of~~ of the dielectric constant of ice and of the range precision of the estimate in determining depth (Cavitte et al., 2016).

The slope of each IRH varies from 1 m $km^{-1}$ to 14.7 m $km^{-1}$, which results in a corresponding uncertainty from 0.1 m to 1.5 m for the 91.1 m offset (the distance between the DF drill site and the point of closest approach on the radar profile). For the firn correction, we used AWI's ICE-CT system to measure the density–depth profile in the upper 126 m of the B53 ice core, with an observational error up to 1 % (Freitag et al., 2013)~~, which~~ . This results in an uncertainty of 0.5 m in the firn correction. The depth uncertainty of dielectric constant affected by anisotropy and temperature is taken to be 1 % (Lilien et al., 2021).

The estimate of the range precision is always ~~higher than the resolution (50 m for AWI RES system) for distinct IRHs. It~~ numerically smaller than the vertical resolution, which is determined by the pulse width of the radar waveform, the signal-to-noise ratio (SNR) and the sub-resolution reflector fluctuations~~(Cavitte et al., 2016). Our~~ . The last term could be ignored when the reflectors display a continuity in reflection amplitudes and consequently traceability (Cavitte et al., 2016). In our case, the precision of the range estimate is calculated from the SNR and range resolution. In our case the precision of the range estimate

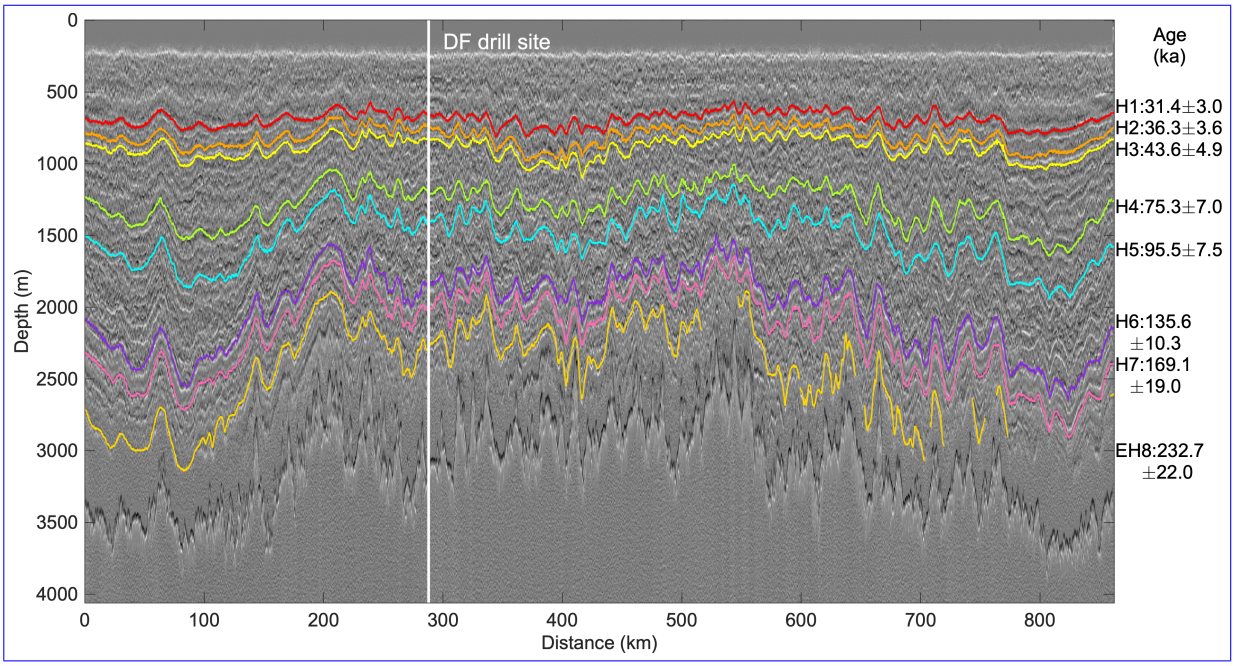


**Figure 2.** Radargram of the profile 20170240. ~~Vertical~~ The vertical white line shows the location of the DF drill site. Lines with different colours represent continuous horizons H1–H7 and the specially traced discontinuous horizon EH8. The dated age and age uncertainty of each horizon is marked on the right.

is almost the same as the range resolution (∼ 25 m), but the precision of the range estimate is actually lower (>50 m) in the deep ice since our radar system has a 50 m pulse width.

The resolution of our system is lower than that of more advanced radar systems, and this causes a smaller number of internal horizons as well as a lower traceability. Moreover, the bedrock topography is characterized by a series of mountain ranges and valleys and wide melting distribution in the Dome Fuji region, which leads to the discontinuity of isochrones at some places, especially near the bottom. Therefore, we need to consider the sub-resolution of different reflectors in our analysis.

We find that the uncertainty caused by the low traceability and continuity is large when we trace the horizons manually. We therefore attempt to trace horizons via several path to circumvent locations where horizons are disturbed or discontinuous. Therefore our best guess for ~~uncertainty for each IRH~~ the uncertainty of each IRH depth is based on continuity and definition during ~~manually tracing,~~ manual tracing. It varies from 20 m to 50 m. ~~Thus, the~~

The overall depth uncertainty varies from 28.5 m to 70.5 m~~in total~~, leading to an age uncertainty range from 2.1 ka to 16.8 ka. The age uncertainty of the ~~ice-core~~ ice core itself is interpolated from the age errors of the agescale DFO-2006 (Kawamura et al., 2007). In total, the age uncertainties range from 3.0 ka to 19.0 ka for the 7 IRHs.

### 2.4 1-D age model

To extrapolate the age–depth profile in the study area below the depth of the deepest IRH, we use a 1-D pseudo-steady ice flow model developed by ~~Parrenin et al. (2006, 2017) but with a simplified constraint~~Parrenin et al. (2006, 2017) but with simplified constraints. This model assumes that the geometry, the shape of the vertical velocity profile and the relative density profile are constant. The real ice age $\chi$ can be calculated ~~from~~ using the steady age $\bar{\chi}$ and the temporal factor $r(t)$ by

$$\bar{\chi} = \int_0^t r(\chi')\mathrm{d}\chi', \tag{1}$$

where $r(t)$ is deduced from the accumulation record of the DF ice core~~,~~. We assume $r(t) = 1$ beyond the extent of the DF ice-core record (715 ka BP), else

$$r(t) = \dot{a}(x,t)/\bar{a}(x), \tag{2}$$

where $\dot{a}$ is the accumulation rate and $\bar{a}(x)$ is the temporally averaged accumulation rate at a certain point $x$. The steady age $\bar{\chi}$ can be ~~inverted~~ inferred from depth $d$ and the layer thickness $\lambda(d)$,

$$\bar{\chi}(d) = \int_0^d \frac{1}{\lambda(d')}\mathrm{d}d'. \tag{3}$$

Assuming that there is no basal melt, $\lambda(d)$, approximated by the Lliboutry model (Lliboutry, 1979), is

$$\lambda(d) = \bar{a}\left(1 - \frac{p+2}{p+1}\left(\frac{d}{H_m}\right) + \frac{1}{p+1}\left(\frac{d}{H_m}\right)^{p+2}\right), \tag{4}$$

where $p$ is a shape factor controlling vertical deformation (Lilien et al., 2021), $H_m$ is the mechanical ice thickness, which ~~means the effective ice thickness above the stagnant ice, and $p$ is a shape factor controlling vertical deformation (Lilien et al., 2021).~~

~~We use a least square optimization to deduce the age–depth profile by varying $\dot{a}$, $H_m$ and $p$.~~ is different from the observed ice thickness $H_{obs}$. The main difference between the model we use here and the one developed by ~~Parrenin et al. (2006) is that we use the mechanical ice thickness $H_m$ instead of a term for the basal thermal conditions. Thus,~~ Parrenin et al. (2006) is that no thermal modeling and thermal boundary conditions are considered here. Instead, we use the ~~inverted~~ inferred $H_m$ to judge if ~~there~~ melting is present or if stagnant (i.e. dynamically irrelevant) ice prevails. When $H_m$ is greater than the observed ice thickness ~~$H$~~ $H_{obs}$, we have melting conditions at the base. Otherwise, there is ~~a basal layer of~~ stagnant ice. If ~~the basal ice is~~ there is basal ice melting, the melt rate $m$ can be obtained by

$$m = \lambda(H_{obs}), \tag{5}$$

We use a Scipy least square optimization to deduce the age–depth profile by varying $\bar{a}$, $H'_m$ and $p'$, where $H_m = e^{H'_m}$, $p = e^{p'-1}$ to prevent $p < -1$ and $H_m < 0$. The minimized cost function is

$$S = \sum \frac{(\chi_i^{iso} - \chi^{mod}(d_i^{iso}))^2}{(\sigma_i^{iso})^2} + \frac{(p'_{prior} - p')^2}{(\sigma^{p'})^2}, \tag{6}$$

where ~~$H_{obs}$ is the observed ice thickness.~~ $i$ is the ordinal number of the IRH, $\chi^{iso}$ is age of the IRH, $\sigma^{iso}$ is the confidence interval on the age, $\chi^{mod}$ is modeled age, and $d^{iso}$ is the depth of the IRH, $p'_{prior} = 3$ and $\sigma^{p'} = 1$ (Parrenin et al., 2007; Chung et al., 2023). The uncertainty of each inverted parameter could be inferred from the optimization and the covariance matrix. To quantify the reliability of the model at each point, we introduced a reliability index $\sigma_R$, i.e., the standard deviation of residuals, ~~$\sigma_R$~~

$$\sigma_R = \sqrt{\frac{R^T r}{n_{iso}}} \sqrt{\frac{R^T R}{n_{iso}}}, \tag{7}$$

where $n_{iso}$ is the number of IRHs, ~~$r$~~ $R$ is the residuals deduced by ~~the age of IRHs $\chi_{iso}$ and modelled age $\chi_{mod}$~~

$$R = \frac{\bar{\chi}_{iso} - \bar{\chi}_{mod}}{\sigma_{\chi_{iso}}} \frac{\bar{\chi}^{iso} - \bar{\chi}^{mod}}{\bar{\sigma}_{\chi^{iso}}}. \tag{8}$$

In this way the model achieves the balance of efficiency and numerical requirements. More details on the model can also be found in the companion paper (Chung et al., 2023).

## 3 Results

Age, age uncertainty of IRHs and temporal variations of accumulation rates at the DF drill from ~~Dome Fuji Ice Core Project Members (2017) are used as input to~~ Dome Fuji Ice Core Project Members (2017) are used to constrain the 1-D steady-state ice flow model. The ~~outputs~~ output variables of the model are accumulation rate $\dot{a}$, shape factor $p$, mechanical thickness $H_m$, age–depth distribution and either basal melt rate or the thickness of the stagnant ice layer.

### 3.1 Modeling results for an ~~exemplary~~ example profile

We integrate 1-D modeling results every 1 km along the ~~exemplary the~~ example profile 20170240, displayed as a cross section through the ice sheet in Fig. 3, to get the 2-D ~~modelled~~ modeled age–depth distribution. We find ice older than 1 Ma along the profile from $\sim$ 150 km to $\sim$ 550 km, where the ice sheet is ~~relatively thin~~thinner than in the other parts. Basal melting is present at the DF drill site and along most parts of the profile, where the mechanical ice thickness $H_m$ (purple dash line) is larger (deeper) than the observed ice thickness (black line).

### 3.2 Age of basal ice

We use 20 ka m$^{-1}$ as a cut-off value for age density of basal ice, beyond which usage of proxies in the ice for paleoclimate reconstruction is currently difficult. This age density corresponds to a full 40 ka climate glacial–interglacial cycle in 2 m of ice. Fig. 4a shows the age of the basal ice (i.e. at the depth of the bed or where the age density reaches 20 ka m$^{-1}$) in the DF region. It varies from 215 ka to ~~2530~~2533 ka. Fig. 4b shows the corresponding depth of the basal ice, which falls in a depth range of 1.6–3.8 km. The age of the basal ice at the DF drill site is extrapolated as ~~1345.8~~1347.2±~~494.3 ka .~~ 503.1 ka at the ice-bed interface. The maximum age of ice at NDF is extrapolated as 1472.1 ka±509.0 ka at depth of 2080.7 m. Fig. 4c shows the age uncertainty of the basal ice, which ranges from 29 to 1050 ka and varies with age of basal ice.

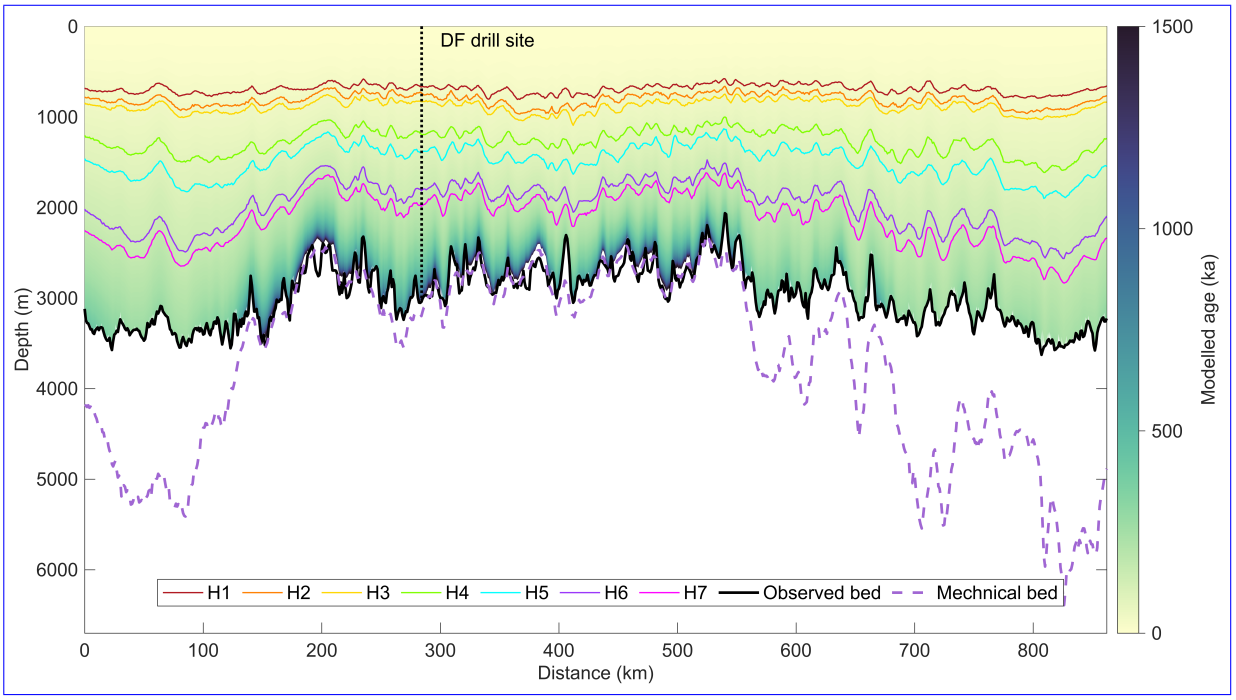


**Figure 3.** ~~Modelled~~ Modeled age–depth distribution of the radar profile 20170240. The coloured lines (see legend) correspond to the traced IRHs shown in Fig. 2. The purple dashed line shows the mechanical ice thickness $H_m$ and the black line shows the bed observed in the radargram. Where the purple dashed line is above the black line, stagnant ice is present and the depth difference between the two lines is the thickness of stagnant ice layer. In other cases, melting prevails.

The age density of ice at 1.5 Ma is shown in Fig 5a, with a range of 6–20 ka $m^{-1}$. It is considered sufficient for paleoclimatic reconstructions (Fischer et al., 2013). This figure also points out the four candidate areas where ice of more than 1.5 Ma old could potentially be found (marked as dark red-dashed ellipses): the first one is a large subglacial mountain range located within a ~100 km radius around the DF drill site; the second one is ~ 160 km to the ~~north-west~~ west of the DF drill site, connected with the first site; the third one is ~ 240 km to the ~~north-west~~ west of the DF drill site and separated from the first two; the fourth one is ~ 260 km to the ~~south-west~~ south of the DF drill site. These fourth potential ~~target~~ candidate areas are all situated in regions with ice thickness of 2200–3000 m, where the ice is not too thick, which would result in basal melting, but still thick enough to ~~include the~~ potentially contain a long-term and sufficiently resolved ~~ice~~ ice-core record. Moreover, these sites, especially the first one close to DF, appear to be distributed ~~along some sort of~~ over high plateaus. This could imply that the ice column here is potentially less disturbed and includes ~~layers~~ horizons of higher lateral continuity.

### 3.3 Basal thermal states

Basal ~~condition is a crucial criterion~~ conditions are crucial criteria for the presence of old ice, because any melting causes ~~ice loss~~ ice loss in the lowermost part of the ice column, which severely limits the age of the basal ice (Fischer et al., 2013).

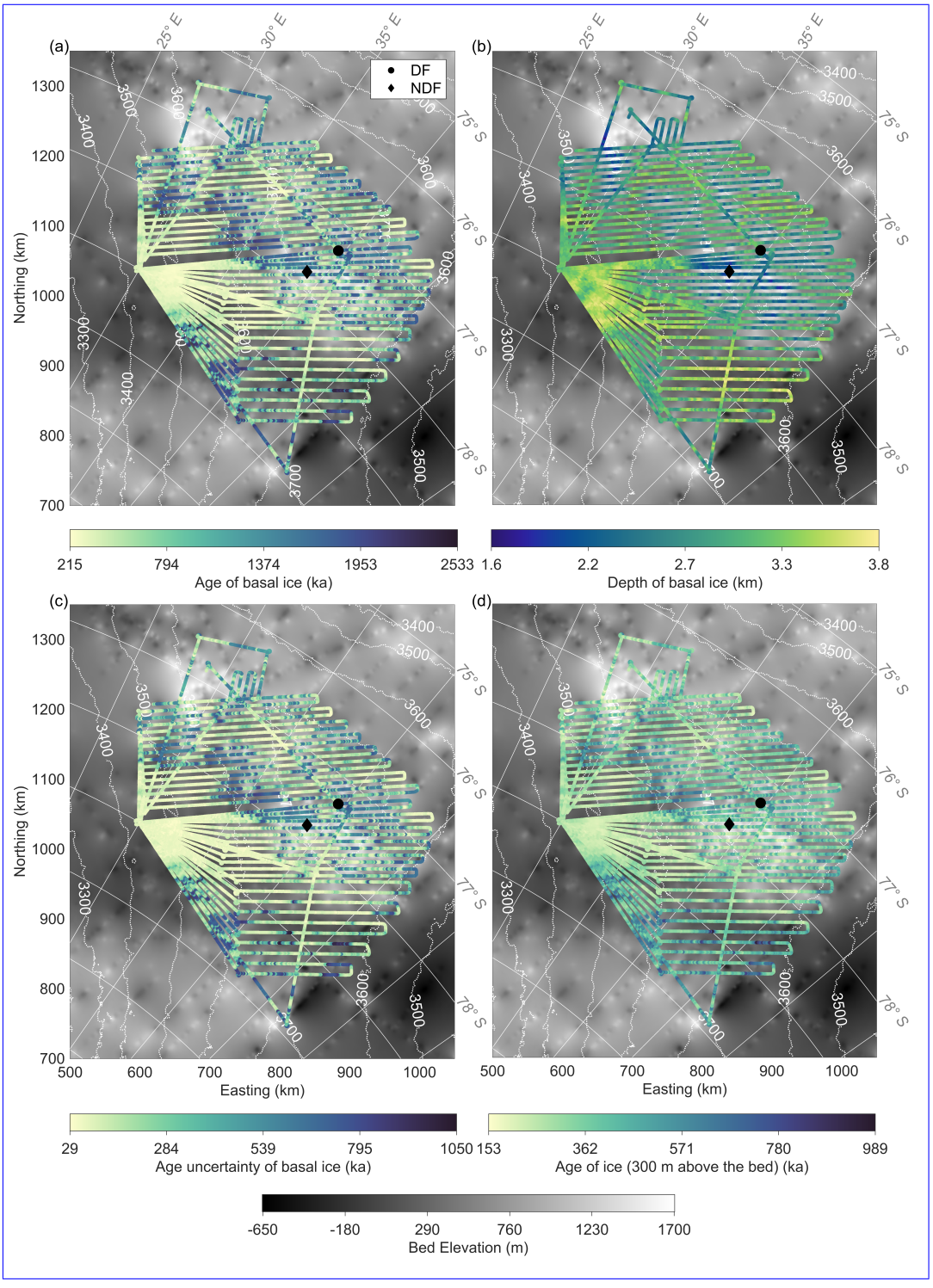


**Figure 4.** (a) ~~Modelled~~ Modeled age of the basal ice at a maximum age density of 20 ka $m^{-1}$. (b) Depth of the basal ice at an age density of 20 ka $m^{-1}$. (c) Modeled age uncertainty of the basal ice. (d) Modeled age of the ice at a height of 250 m above the bed.

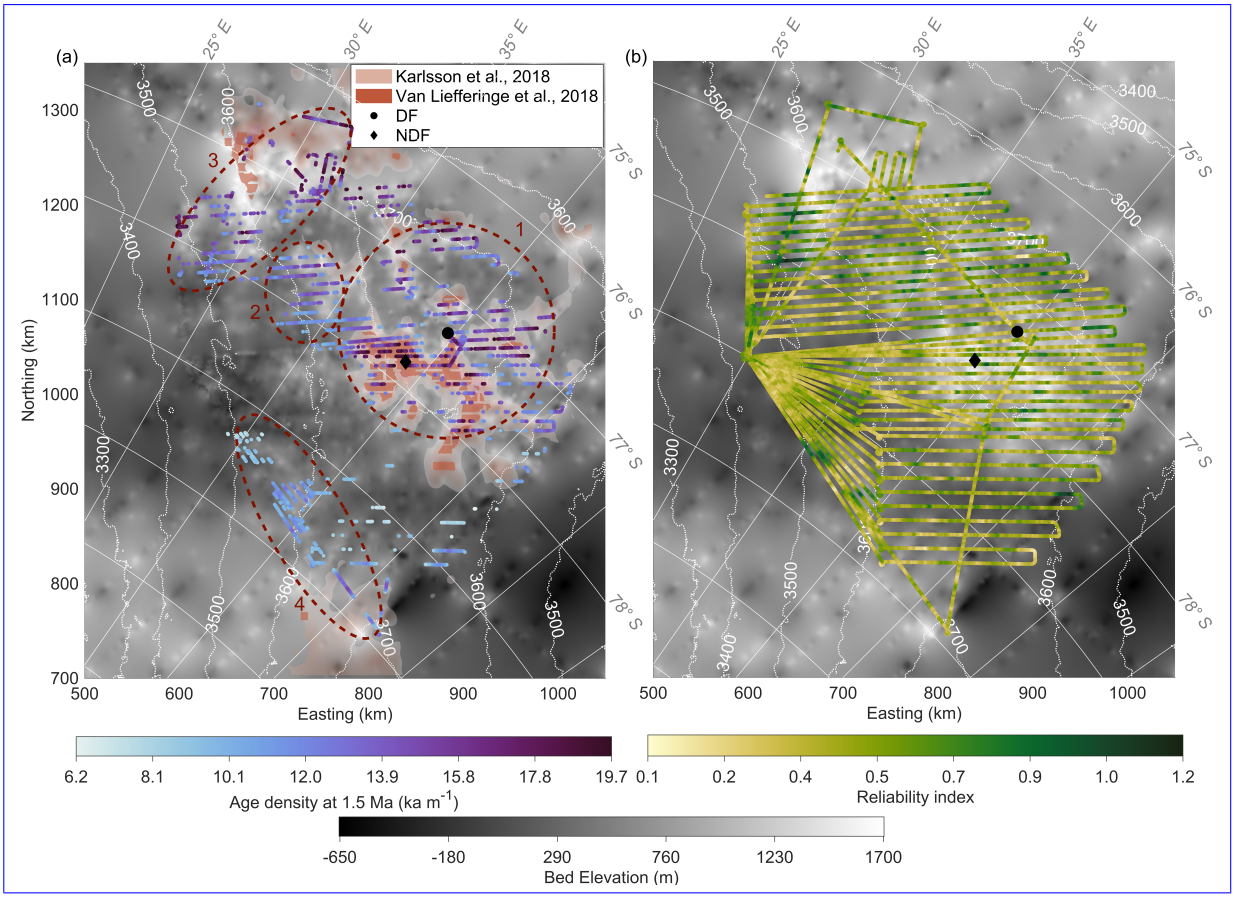


**Figure 5.** (a) Age density of ice at 1.5 Ma, the dark red ellipses show the potential old sites considering basal age and age density. Semi-transparent pink-red colored shades show potential old-ice sites suggested by ~~Karlsson et al. (2018)~~Karlsson et al. (2018)—the deeper the color~~is~~, the higher the possibility of old ice. The ~~gray~~ orange shades show the ~~old ice site~~ old-ice sites suggested by ~~Van Liefferinge et al. (2018)~~Van Liefferinge et al. (2018). (b) Reliability index ($\sigma_R$) map in the DF region, the reliability of the model output decreases with decreasing reliability index ($\sigma_R$) increasing.

From our model we also ~~get~~ obtain the basal conditions, including melt rate or stagnant-ice thickness (Fig. 6a). According to our results, basal melting prevails over frozen conditions with the formation of stagnant ice in the survey area. ~~Modelled~~ Modeled basal melt rates vary from 0 to ~~8.40~~8.39 mm $a^{-1}$. Melting is significant $\sim$ 200 km ~~west~~ south-west and $\sim$ 150 km ~~south~~ south-east of DF, where we observe ice thicker than 3000 m, i.e. ice thick enough for the temperature to reach the pressure melting point. The basal melt rate at the DF drill site is interpolated as $0.11 \pm 0.37$ mm $a^{-1}$.

Stagnant ice has a thickness range of 0–400 m. Two clusters of stagnant ice are distributed $\sim$ 60 km south-west (~~around~~ immediately north of NDF) and $\sim$ 180 km ~~north-west of the~~ west of DF (in the second ~~old ice candidate ).~~ old-ice candidate site). The thickness of stagnant ice is modeled as 206.5 m at NDF. Our results show that melt rates are generally higher in subglacial basins and lower (or even frozen conditions) in subglacial mountainous terrain.

### 3.4 Accumulation rate

Accumulation rate is another important factor for the age distribution. We show the temporally averaged (over 720 ka) accumulation rates in the DF region from our model results in Fig. 6b~~, they~~ . They vary from 0.015 to 0.038 m $a^{-1}$ ice equivalent. At the DF drill site, the accumulation rate spatially interpolated between the radar lines is 0.022 m $a^{-1}$. In the ~~large~~ larger DF region, it shows a ~~north–south~~ west–east decreasing gradient.

~~(a) Modelled stagnant-ice thickness and basal melt rate along the profiles of the radar survey: blue represents stagnant ice thickness and red represents the melt rate. Dark blue lines are subglacial lakes deduced from basal reflectivity in radargrams by Karlsson et al. (2018). (b) Modelled averaged accumulation rate in ice equivalent along the profiles of the radar survey.~~

In the Supplement ~~Figs~~Fig. S1 we also show the shape factor map in the DF region obtained from the model.

## 4 Discussions

### 4.1 Age of ice: comparison with previous studies

There is signifant uncertainty in the basal age of ice over the entire DF region. We relate this phenomenon to the fact that the number and depth of IRHs used as constraints for the model are limited by their traceability in our radar data set. IRH constraints help to determine the shape of the thinning function ($p$ factor), therefore, using more IRHs gives a more accurate $p$ value. The thinning function is almost linear in the upper section of the ice sheet and then becomes non-linear in the deepest part. Since the IRHs we have traced are located in the top two thirds of the total ice thickness, we cannot constrain the model well in the lower third. However, this lower section has the largest impact on the $p$ value. For comparison, in the Dome C region, the age uncertainty of each IRH is similar to that in the DF region and Chung et al. (2023) adapted the same model approach, but the modeled age uncertainty of basal ice is much smaller in the Dome C region. This is likely due to more IRH constraints covering a larger portion of the ice sheet thickness in the DC region. We consider this comparison important, as the same approach applied in different regions and/or to different radar data set can yield a considerably different uncertainty.

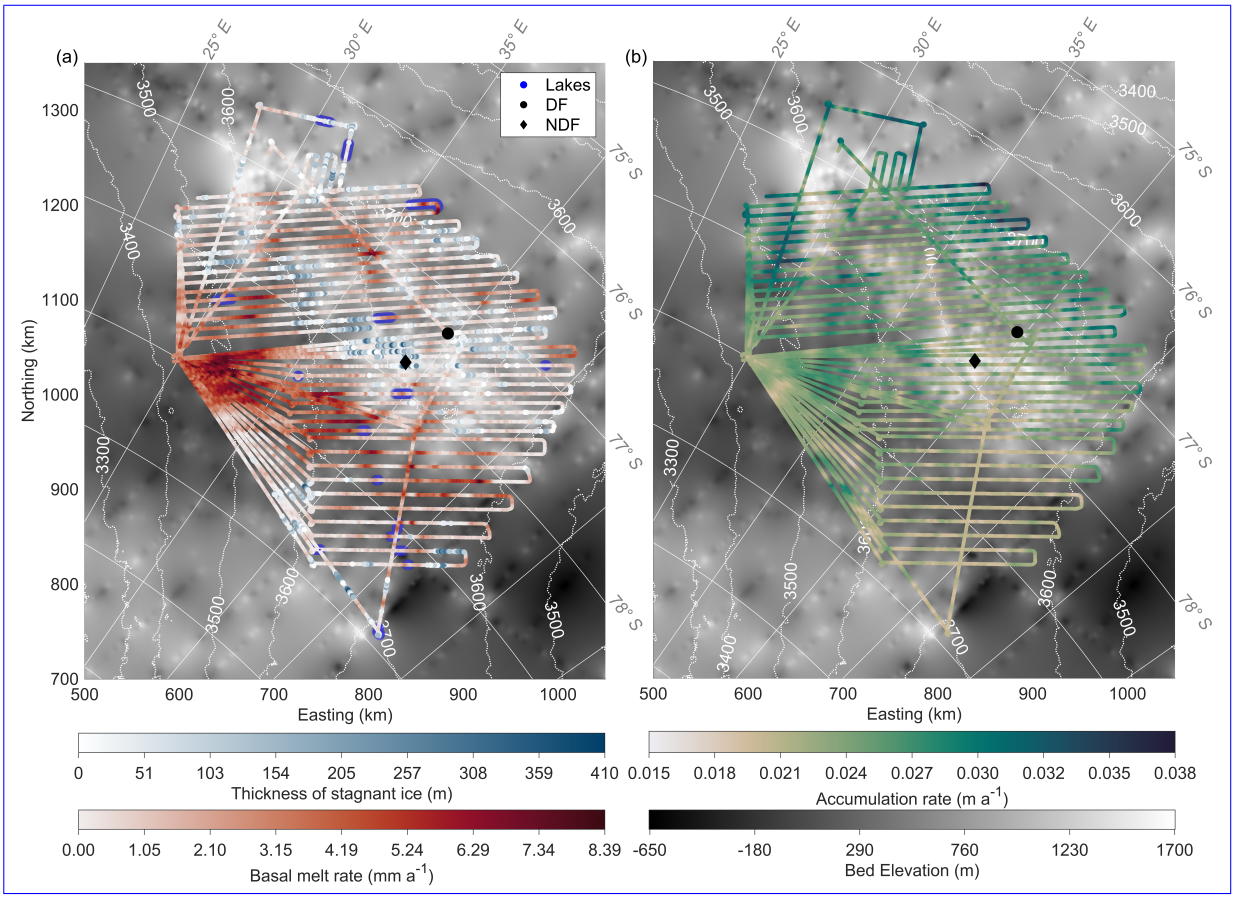


**Figure 6.** (a) Modeled stagnant-ice thickness and basal melt rate along the profiles of the radar survey: blue represents stagnant ice thickness and red represents the melt rate. Dark blue lines are subglacial lakes deduced from basal reflectivity in radargrams by Karlsson et al. (2018). (b) Modeled averaged accumulation rate in ice equivalent along the profiles of the radar survey.

Several previous studies have already investigated the potential age of basal ice either at the DF drill site or its surrounding region. At the DF drill site, ~~Parrenin et al. (2007)~~ Parrenin et al. (2007) proposed that ice more than ~~several million yeas~~ a million years old could exist near the ice–bed interface, according to the results of ~~a~~ their 1-D ice flow model. ~~Hondoh et al. (2002)~~ Hondoh et al. (2002) deduced chronologies of the DF ice core based on the correlation between the local metronomic signal (Milankovitch components of the past surface temperature oscillations) and ~~isotope record, and~~ the isotope record. They then extropolated this timescale to 3050 m depth ~~by~~ using a simplified ice-flow model. Their result suggested that age may reach 2000 ka at about 3000 m depth at the DF drill site. These two results correspond approximately to ~~our inverted~~ the range of our inferred bottom age of ~~1345.8~~1347.2±~~494.3~~503.1 ka at ~~3034.1 m~~the ice–bed interface (∼ 3050.5 m).

~~?~~ Obase et al. (2023) used a 1-D ice flow model, which computes the temporal evolution of the vertical age and temperature profiles. They also extended their modeling results along a DF–NDF radar transect from DF to NDF, where the basal ice has

a tendency to be older. They used ground-based radar data from the JARE59 survey (2017–2018) ~~in~~ which covered an area of approximately 120 km × 100 km ~~, collected in~~ with a dense grid ~~by~~ of radar lines. The data was collected using an incoherent pulse-modulated VHF radar sounder with a peak transmission power of 1 kW, transmitter pulse widths of 60 ns and 250 ns, which corresponds to a pulse-limited vertical resolution of 5 m and 21 m, respectively. In addition, ~~the model they used is a transientmodel considering~~ their model is transient, therefore age and temperature both change with time. It estimates the age through the vertical advection equation ~~,~~ and uses the GHF as the basal boundary condition, while we use a 1-D steady model, which calculates the age through an analytical thinning function and excludes all thermal modeling by introducing a mechanical ice thickness.

Despite the differences in the radar data characteristics of the JARE59 and AWI surveys and slightly different models, the results are reasonably consistent. We estimate the age of the basal ice at DF to be ~~841.8 kaand 1034.5 ka at 100 m and 50 m above the bed, respectively, while ? extrapolated them as 880 ka and 1250 ka, respectively~~1347.2±503.1 ka, while Obase et al. (2023) extrapolated it as a range of 400–1000 ka with a GHF in the range of 60–52 mW $m^{-2}$, respectively, in their Fig. 6a. In addition, our results confirm that the age of the basal ice is getting older from DF to NDF.

The two previous studies by ~~Karlsson et al. (2018) and Van Liefferinge et al. (2018)~~ Karlsson et al. (2018) and Van Liefferinge et al. (20 are based on a ~~thermodynamical~~ thermodynamic model, considering regions with an surface ice flow velocity smaller than 1 m $a^{-1}$. Their main constraint for the presence of old ice is that the GHF is not sufficiently large to cause temperate conditions at the base, and thus melting. Another criterion is ice thicker than 2000 m and 2500 m~~respectively.~~ , respectively. They suggested several potential areas holding old ice, which are displayed by semi-transparent pink and orange shades in Fig. 5, respectively. Our approach, in contrast, is solely based on the observed age–depth distribution, which is then extrapolated to larger depth by using observed accumulation rates and making assumptions about the thinning function. ~~The semi-transparent shades in Fig. 5a show the potential areas with old ice, suggested by Karlsson et al. (2018) and Van Liefferinge et al. (2018). The shades are to a large degree concurrent to~~

The model we are using does not take into account the thermodynamics at all, thus it is more independent of GHF estimates. However, the sites with potentially "old ice" suggested by the above mentioned two different approaches show a considerable correspondence in some places with our results, especially ~~to~~ at the first candidate (a large subglacial mountain range located immediately around the DF drill site)~~, although the approaches are very different~~. We consider that the two main underlying reason for this consistency is the use of ice thickness in both models, which has implied the important impact of ice thickness on the age distribution of the ice, as well as the validity of the approximations regarding the thinning function in our approach.

### 4.2 Basal thermal state and accumulation rate: comparison with previous studies

A spatial comparison between our result and subglacial lakes identified previously by ~~Karlsson et al. (2018)~~ Karlsson et al. (2018) in Fig. 6a shows that ~~we find~~ all 16 lakes are located in regions where we obtain basal melting, and in 11 lakes we can observe significant melting.

~~Basal~~ The basal melt rate is a parameter impacted by the spatial distribution of GHF, which is a regional ~~value~~ parameter and also can show strong variations on the local scale, depending on topography (Colgan et al., 2021). ~~Regarding the local~~

~~characteristic of GHF~~ By averaging the local GHF variations, we calculate regionally ~~averaged~~ melt rates in different areas around the DF drill from our results for the comparison with previous basal melt ~~rate~~ rates at DF. In our ~~result,~~ results, the mean basal melt rates increase with the ~~further distance to~~ distance from the DF site (i.e., in a larger region).

~~At~~ Using a 1D ice flow model at the DF site, ~~Parrenin et al. (2007) suggested that with a probability of 90 %~~ Parrenin et al. (2007) suggested that the basal melt rate is ~~smaller than~~ < 0.2 mm $a^{-1}$ ~~through 1D ice flow model. Seddik et al. (2011)~~ with a probability of 90 %. Seddik et al. (2011) deduced a basal melt rate of $\sim$ 0.35 mm $a^{-1}$ assuming a GHF of 60 mW $m^{-2}$. ~~? got the conclusion of no melting~~ Obase et al. (2023) suggested that there is no melting at DF for a GHF < 56 mW $m^{-2}$ and the melt rate rises to $\sim$ 0.4 mm a when GHF equals 58 mW $m^{-2}$. These three results all agree with our mean basal melt rate of 0.16$\pm$0.37 mm $a^{-1}$ within 5 km around DF. ~~?~~

Obase et al. (2023) also simulated a basal melt rate ~~changing from 1~~ change from 0.6 to 1.5 mm $a^{-1}$ for a GHF increasing from ~~57 to 58~~60 to 64 mW $m^{-2}$ ~~, which corresponds with~~ in their Fig. 5. This corresponds to our averaged basal melt rate of 1.36$\pm$0.69 mW $m^{-2}$ within 200 km around the DF site. ~~Talalay et al. (2020)~~

Talalay et al. (2020) estimated a basal melt rate of 2.5$\pm$0.5 mm $a^{-1}$ at ~~the~~ DF based on the temperature profile ~~from~~ measured in the ice-core borehole and ~~applying~~ an analytical solution to infer the vertical velocity. This value is consistent with our mean basal melt rate of 1.67$\pm$0.76 mm $a^{-1}$ in the entire DF region. However, this value is very different from our estimate at the DF drill site ~~and probably~~ and—despite potential shortcomings in their approach—probably closer to reality. In Section 4.3.3 we discuss the ~~possibility of~~ possible overestimation of the ~~age of the basal ice due to the~~ basal ice age due to an inflection point at the bottom ~~part~~ of the timescale, ~~and therefore we may~~ which would mean that we underestimate the basal melting. ~~We show the detailed~~ Figure S2 shows the mean value and standard deviation of the basal melt rates within different distances ~~to~~ of the DF drill~~in Figs. S2.~~.

In the ~~large~~ larger DF region, ~~the~~ model-derived stagnant ice is ~~present in only~~ only present along 8 % of the ~~area along the~~ radar profiles, and has an average thickness of 95.6 m. The distribution of the stagnant ice implies that the region immediately north of NDF is the area most likely to have a cold bed which could hold old ice in the DF region. Our companion paper shows that in the DC ~~region~~ and LDC region, the basal thermal states are very different. Stagnant ice prevails over melting in the DC area and it dominates the LDC region, with a thickness of up to 250 m (Chung et al., 2023). The relatively warm basal thermal condition in the DF region ~~is a negative factor for holding the old ice .~~ make it less likely that old ice exists. Complementary to our model results, other studies have found some evidence of stagnant ice in radargrams as notable events, e.g., no continuous or coherent reflecting horizons (Lilien et al., 2021) or diffuse scattering (Cavitte, 2017) in radar detection range. However, in the radar data set we use, there is an echo free zone (EFZ) above the bed, with a thickness of several hundreds of meters. There are various possible causes for an EFZ, e.g., sensitivity of the radar system, deformation, folding or recrystallization of ice (Drews et al., 2009; Franke et al., 2023). We consider that the EFZ in our data set is most likely caused by the performance of the radar system, as in the same region more modern systems can detect somewhat deeper, more coherent horizons (Rodriguez-Morales et al., 2020). Therefore, we could not observe any unambiguous evidence of stagnant ice in our radargrams. Fujita et al. (2012) found no features in their radar observations that could be interpreted as evidence of the refreezing basal water. They attributed this to the relatively smaller variations in bedrock topography and thus ice thickness

in the DF area compared to other regions in Antarctica, where basal freeze-on was proposed. Basal melt water would thus favorably drain downstream in the DF area than to follow paths which would enable local freeze-on locally.

In the DF region, ~~Fujita et al. (2011)~~ Fujita et al. (2011) showed an map of accumulation rate with a decreasing trend from 76° S to 78° S, which is consistent with the distribution of accumulation rate in our result.

### 4.3 Reliability and sensitivity study of the 1-D model

#### 4.3.1 Reliability of the model

Our 1-D model does not consider horizontal advection, which, although low near an ice divide, exists away from the divide. In these places, the reliability of the model ~~could be relatively~~ is lower. We show the reliability index ~~in~~ $\sigma_R$ (described in Section 2.4) in the DF region (Fig. 5b). A smaller reliability index $\sigma_R$ represents higher reliability of the model. The reliability index $\sigma_R$ ranges from 0.1 (reliable) to 1.2 (less reliable) in the DF region. ~~We find that in the northern part of the DF region, the model is relatively less reliable.~~ The distribution indicates a relatively ~~high~~ higher reliability in the DF region compared to that in the DC region (0–2) (Chung et al., 2023). The reliability of the model in the DF region could be overestimated because of the limited number and depth of IRHs.

To evaluate the reliability of the model results in ice deeper than the available IRHs, we also determine the spatial deviation of the age of basal ice ~~in different distances to the DF /~~at different distances from DF and NDF as a function of normalized ice thickness. The ~~spreading of the age of basal~~ underlying assumption is that the age–depth function should be rather similar for the same (normalized) ice thickness within a region for small flow velocities and where the overall ice dynamic behaviour (e.g. prevailing divide or flank flow regime) is comparable. The spread of the distribution of age of deep ice, shown in Table 1, generally increases with distance from DF ~~/~~and NDF, except between 100 and 200 km distance from both sites and >200 km from NDF. The distribution of the age–normalized depth is illustrated in Fig. S3 in the supplement.

We interpret the larger spread to reflect the increasing transition from a dome-flow to a flank-flow regime. Within the region of clear characteristic of divide flow, i.e. a relatively smaller spread, implies that it is ~~reasonably adequate~~ reasonable to apply a 1-D model. Our approach is comparable to the ~~constraint~~ method mentioned above used by ~~Karlsson et al. (2018) and Van Liefferinge et al. (2018)~~ Karlsson et al. (2018) and Van Liefferinge et al. (2018) to investigate the age only in areas with an ice flow velocity $< 1$ m a$^{-1}$ (in ice equivalent). The standard deviation ~~in age~~ of the age distribution 5 km around NDF (~~47.9~~50.9 ka) is much smaller than that around DF (~~392.3~~392.7 ka)~~, which~~ . This could tentatively be interpreted as flow characteristics near NDF ~~being closer to~~ representing more homogeneous divide flow than those at DF. ~~We show the distribution of the age–normalized depth in Figs. S3 to evaluate the flow regime further.~~

~~We then design sensitivity studies to~~

#### 4.3.2 Sensitivity study

We next discuss sensitivity studies with which we investigate how different ~~inputs~~ data inputs and constraints affect the model and how the reliability of the model could be improved.

**Table 1.** Spatial standard deviation of age of basal ice ~~in~~ at different distances ~~to~~ from DF and NDF.

| | Standard deviation (ka) | |
|---|---|---|
| Distance (km) | Around DF | Around NDF |
| < 5 | ~~392.3~~ 392.7 | ~~47.9~~ 50.9 |
| 5–15 | ~~486.9~~ 487.0 | ~~368.2~~ 369.3 |
| 15–50 | ~~526.0~~ 526.5 | ~~528.8~~ 529.6 |
| 50–100 | ~~530.5~~ 531.2 | ~~545.0~~ 545.7 |
| 100–200 | ~~497.0~~ 497.7 | ~~517.0~~ 517.7 |
| > 200 | ~~534.2~~ 534.9 | ~~534.7~~ 535.5 |

#### 4.3.3 ~~Sensitivity study~~

The thinning function and the normalized age–depth scale have a stronger gradient in deeper ice than at shallower depths~~, therefore~~ . Therefore the deepest horizon as well as the underlying age–depth scale may have an effect on our modeling ~~result~~results, including shape factor $p$, accumulation rate $\dot{a}$, mechanical ice thickness $H_m$, and age of basal ice $\chi_b$. To investigate ~~either effect~~ these effects, we perform two sensitivity experiments for the profile 20170240.

Our first run corresponds to ~~our~~ the standard model run (STD) which we have been discussing so far, i.e. it uses six or seven ~~IRHs tracked~~ traced IRHs and DFO2006+AICC2012 as the timescale. The timescale provides the ~~information of the age of the IRHs and~~ temporal variations of ~~accumulation rates at DF .~~ the accumulation rate at DF and allows us to date the IRHs.

The second model run (RUN II) investigates the impact of ~~different numbers~~ using a different number of traced IRHs to constrain the model. In order to ~~extend our available age–depth scale to larger depth~~give a better constraint, an extra deeper discontinuous eighth horizon, EH8 with an age of 232.7 ka, ~~is~~ was traced (Fig. 2). As this IRH is discontinuous in the study region, it could not be used reliably on all other ~~profiles.~~ radar profiles, but still provides a useful addition on those profiles where it is present.

In the third run (RUN III), we analyze how different timescales influence the modeling ~~result~~results. We use ~~DFGT-2006 to~~ IRHs H1–H7 from the standard run as constraints, but replace DFO2006+AICC2012 ~~.~~ with DFGT-2006~~is the timescale which reconstruct the age of ice above bed by a 1-D flow model based on~~ . Parrenin et al. (2007) reconstructed the age from the first DF ice core ~~(Parrenin et al., 2007). Since the temporal variations of accumulation rates below~~ using a 1-D flow model, referred to as DEGT-2006. Below 2503 m (the depth of the first deep ice core), the temporal variations of accumulation rate could not be as reliably reconstructed in DFGT-2006 ~~were~~ as for other ice cores, as it was derived from marine cores. Therefore, to increase reliability, ~~which are not reliable,~~ we use the temporal variations of accumulation ~~rates~~ rate below 2503 m from timescale DFO2006+AICC2012 as a replacement. ~~We use the agescale with the seven IRHs from the standard run.~~

~~We~~ In order to quantify the difference between model results from different runs, we provide statistic values of relative percentage difference of shape factor ~~$\Delta p$ %~~$\Delta p$, accumulation rate $\Delta\dot{a}$, mechanical ice thickness $\Delta H_m$, and age of basal ice

**Table 2.** Mean value and standard deviation of relative percentage difference between model runs for the profile 20170240.

| | $\Delta\chi_b(\%)$ | | $\Delta p(\%)$ | | $\Delta\dot{a}(\%)$ | | $\Delta H_m(\%)$ | |
|---|---|---|---|---|---|---|---|---|
| | Mean | Std. dev. | Mean | Std. dev. | Mean | Std. dev. | Mean | Std. dev. |
| STD–RUN II | ~~14.58~~ 14.60 | ~~14.69~~ 14.70 | 12.55 | 10.07 | 0.83 | 0.71 | 4.35 | 3.34 |
| STD–RUN III | ~~10.35~~ 10.43 | ~~10.71~~ 10.63 | 9.07 | 6.09 | ~~3.11~~ 3.20 | 0.18 | 3.15 | 0.60 |

$\Delta\chi_b$ along the profile 20170240 between STD and RUN II, STD and RUN III in Table 2, respectively~~, to quantify the difference between model results from different runs .~~. In the following paragraphs we discuss the results. For extended illustration we refer to the supplement, where we provide and analyse the model results for all three runs Fig. S4 and relative percentage difference of model results between STD and RUN II/RUN III in Fig. S5.

The outcome of RUN II shows that the age of the basal ice and the shape factor are ~~affected severely~~ severely affected by an extra IRH ~~with mean $\Delta p$ % of 12.55~~(mean $\Delta p = 12.55$ % and mean ~~$\Delta\chi_b$ % of 14.58 %~~ $\Delta\chi_b = 14.60$ %). In some regions, EH8 has a somewhat different shape ~~with the uppermost~~ to the upper seven IRHs and thus ~~largely changes the inversion of~~ changes the inferred shape factor and thinning function of ~~every 1-D model, which will lead~~ each modeled point, which leads to significant change ~~of~~ in the age of basal ice. Between STD and RUN III, the mean relative difference of age of the basal ice and the shape factor are also large (~~10.35~~10.43 % and 9.07 %)~~, they~~ . They thus prove the importance of using the most reliable ~~timescale of the ice core. Without the impact of the EH8, the~~ ice-core timescale. The standard deviation of ~~$\Delta p$ % and $\Delta\chi_b$ % are still~~ $\Delta p$ and $\Delta\chi_b$ are significant (6.09 % and ~~10.71~~10.63 %), which could be ~~relevant~~ related to the changes in subglacial topography.

~~$\Delta\dot{a}$ % between STD and RUN II /~~The relative percentage difference $\Delta\dot{a}$ (absolute values) of STD minus RUN II and RUN III has a mean value of 0.83 % and ~~3.11~~3.20 %, respectively, which implies the accumulation rate is almost unaffected by adding an extra IRH and affected more by the timescale. The standard deviation of ~~$\Delta\dot{a}$ %~~ $\Delta\dot{a}$ between STD and RUN III is low (0.18 %), ~~proves~~ which proves that the relative difference ~~is stable~~ seems less variable along the profile. ~~So~~ We therefore suggest that using different temporal variations of accumulation rates at DF could be the main reason for the difference of the modeled accumulation rate between STD and RUN III. This is, however, not surprising, as accumulation ~~is more influenced by changes in the near-surface regions and less by changes at large depths (e.g. an additional constraining IRH)~~ has a larger influence on isochrones near the surface and a smaller influence on the ones at larger depth (Sutter et al., 2021).

Mean values of the relative change in the mechanical ice thickness $\Delta H_m$ imply that both, the number of IRHs (4.35 %) and change of agescale (3.15 %) have a comparatively small impact on the deduced mechanical ice thickness~~, which means~~ . This implies that the mechanical ice thickness obtained from our model is relatively robust compared to other quantities.

~~We show and analyse the model results for all three runs in Figs. S4 and relative percentage difference of model results between STD and RUN II/RUN III in Figs. S5.~~

### 4.3.3 Comparison of the age–depth scales

Comparing the age–depth distribution at the DF drill site of the three model runs (Fig.7), we find that at depths ~~above~~ larger than ∼ 2500 m, the three runs have very similar age–depth scales.

~~The difference~~ The differences between STD and RUN II ~~/~~and RUN III are much larger below a depth of 2500 m, where STD has an age of basal ice of ~~1345.8~~1347.2±~~494.3 ka, RUN II has an extra layer and a resulting~~ 503.1 ka. RUN II with an extra horizon results in an age of the basal ice of ~~1956.1~~1958.0±~~716.8 ka,~~ 726.1 ka, while RUN III uses the input from a different timescale and obtains an age of 1933.7±~~751.9~~769.3 ka at the ~~ice–bed interface~~basal ice. This comparison shows that both, the number of IRHs and the agescale, have a significant influence on age of the basal ice. Since RUN III uses the extrapolated timescale (DFGT2006), not the timescale of the second DF deep ice core determined by ice-core analysis (DFO2006+AICC2012), we will not consider it further in the discussion.

~~Comparing the modeling result of~~ If we only focus on the age of basal ice, it seems that both modeled ages (STD and RUN II~~with their timescale from the DF icecore~~ ) deviate from their timescale DFO2006+AICC2012. The modeled age of STD even seems more reasonable than the modeled age of RUN II with one less IRH, although it is important to note that there is huge uncertainty for Run II and STD. However, since we cannot simply and independently assess the quality of the model results based only on the age of basal ice, we will next analyse the complete age–depth profiles and discuss the age–depth distribution of each RUN.

Comparing the modeled ages of STD and RUN II with their timescale (DFO2006+AICC2012), we find that above ∼ ~~2300~~2350 m, both modeling results have good ~~correspondence~~ agreement with the timescale. From ∼ ~~2300~~2350 m to ∼ ~~2750~~2745 m, only the modeled age of the RUN II agrees with ~~DFO2006+AICC2012. Below~~ the timescale. The STD modeled age is numerically smaller than the age from the timescale, the difference between them increases with the depth. This finding shows the significant impact of the extra IRH EH8 in RUN II: with one more IRH which is 257 m deeper and 63.6 ka older than the one above, the modeled age stays comparatively accurate for a further ∼ ~~2750 m, modeled age keeps the exponential relation with depth but the real~~ 395 m in depth.

RUN II has a reasonable performance down to a depth of ∼ 2745 m, where the age is modeled as 536.4 ka BP. This depth is ∼ 300 m above the bed, which is exactly the depth of the inflection point in the timescale DFO2006+AICC2012~~starts deviating from it. Thus, modeled age has a much larger age gradient~~ . Below this depth, the age–depth profile of the model keeps following the exponential distribution as a model assumption, but the timescale of ice core shows a curvature reversal. Thus, the modeled age gradient is steeper in the same depth range, which leads to ~~an overestimation~~ the large overestimation of the age of basal ice by a factor of two ~~of the age of basal iceat this case. This implies deeper IRHs below 2750 m at this case will have a positive impact on the modeling result as they can provide important real-age constraints~~ in this case. Fig. 4d depicts the spatial distribution of age of ice at 300 m above the bed. It provides relatively accurate age values while excluding the lowest part of the ice. The age has a range of 153 ka–989 ka, and implies that there is a small area for old ice at this depth ∼ 200 km south–east to DF.

Obase et al. (2023) shows this inflection at the same depth (∼ 300 m above the bedrock) in their Fig. 6a, and it also caused a much older modeled age compared to the observation. Such an inflection point in the age–depth scale obviously indicates that the underlying analytical assumption for our model approach is less valid below its depth of occurrence.

A similar phenomenon was also observed in our companion study with the same model approach (Chung et al., 2023) at EDC, though much older IRHs (up to 476.4 ka BP) were dated there. They pointed out that the modeled age at the deepest dated point for the EDC drill site was around 100-200 kyr older than would be expected from the AICC2012 age–depth profile. The reason could be that the profile of the timescale AICC2012 determined by ice-core analysis does not follow an exponential profile in the lower 200 m of dated ice. Since the timescale of EDC does not change as drastically as that of DF ice core near the bedrock, the overestimation of the modeled age of basal ice at EDC is not as significant as that at DF. For illustrative purposes we also show the model derived age–depth scale and AICC2012 timescale at EDC in Supplement Fig S6.

To solve this overestimation problem in the case of DF, only more continuous isochrones below the inflection point, i.e., the lowest 300 m, would provide better constraint for the model. ~~Considering the overestimation we observe at the DF drill, the reliability of our model is probably overestimated~~This is not possible with our radar data set and is also unlikely to be easily achievable in other data sets (e.g. Tsutaki et al., 2022).

The logging of the DF borehole and the drilling process indicated melting at the base of DF (Motoyama et al., 2021), which could be one reason for the inflection point in the timescale of the ice core. This would imply that the significant overestimation likely occurs in areas with basal melting. Given that there is only one deep ice core in the DF region, we lack an additional timescale extending towards the bedrock to prove our hypothesis. Whether the inflection point in the age–depth profile is a general feature in the DF region is still an open question.

Overall, we find that our model works quite well in the upper two thirds of the ice column according to the calculated reliability index (the standard deviation of the age difference between observation and model results). It also seems appropriate in the deeper part of the ice column at DF, down to the depth of the inflection point of the timescale. Since we have found that areas of basal melting prevail over those with stagnant ice in the DF region, it is possible that overestimation of age occurs in the deep ice at various places, as what was already observed at DF. Taking this into consideration, we emphasize the importance of considering the basal thermal state for locating old ice, i.e., more attention should be paid to areas indicating the presence of stagnant ice.

#### 4.3.4 ~~Limitations of radar system~~

### 4.4 Limitations of radar system and model

In the following we will discuss the current limitations from the perspectives of the radar system and the model, respectively, in order to point out potential improvements for future approaches.

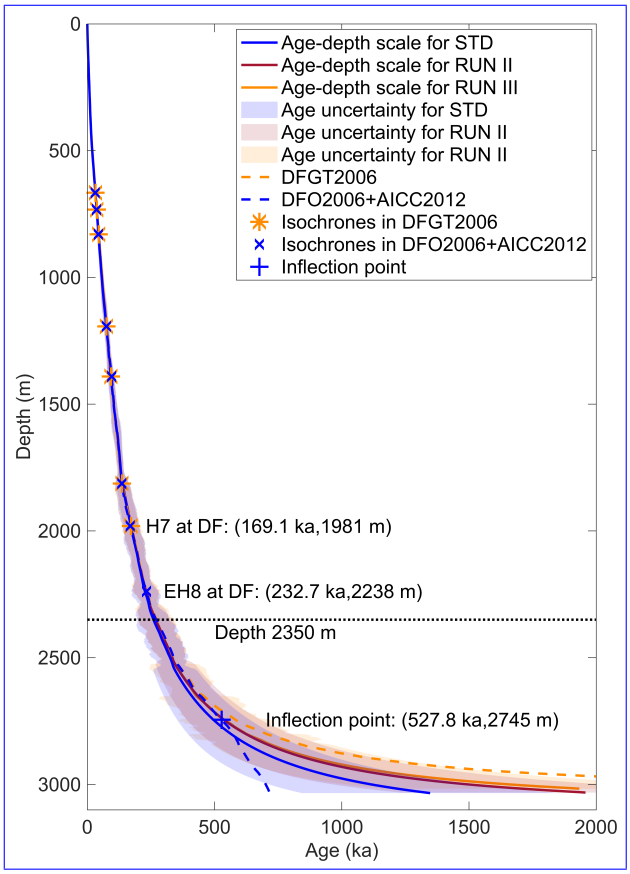


**Figure 7.** Comparison of age–depth scales of three models (solid lines), their uncertainties (shades) and two timescales from the DF ice core (dashed line). Note that the uncertainties of RUN II and III are similar, so their shades are overlapped mostly. The asterisks and crosses show the age and depth of IRHs for the DFGT2006 and DFO2006+AICC2012 timescale, respectively. The plus sign shows the inflection point of the timescale DFO2006+AICC2012. Labels at the distribution indicate horizon, age and depth.

### 4.4.1 Radar system limitations

According to the sensitivity study and comparison of age–depth scales, the shape of IRHs (i.e., the accuracy of tracing) and the depth of IRHs have ~~significant impacts on the modelled~~ a significant impact on the modeled age of the ice. However, compared to modern state-of-the-art radar systems, the data collected ~~with~~ by the AWI RES system ~~has a lower resolution~~ with a pulse width of 50 m, ~~which~~ leads to marked ~~errors during manual IRHs picking~~ higher uncertainties during manual IRH tracing and thus lower reliability of ~~modeling results.~~ the model results. The lower resolution and SNR also limits the number of traceable IRHs, which in turn increases the age uncertainty in the bottom part of ice. In addition, although we ~~pick~~ traced the deepest continuous ~~layer with an age of~~ horizon at 169.1 ka in this study, ~~there is still more than one~~ the lowermost third of the ice column ~~in the lowermost part that is not dated~~is still not dated yet. The lack of ~~signal~~ clear coherent return signals in

lowermost part likely originates not only from ~~ice dynamics~~ the physical properties of the ice but also from the limitations of the radar system. ~~Rodriguez-Morales et al. (2020) showed~~ Rodriguez-Morales et al. (2020) investigated the comparison of data collected ~~by~~ with the ground-based CReSIS' UWB radar, ~~NIPR radar and our AWI 's airborne~~ Japanese National Institute of Polar Research (NIPR) radar and the AWI RES system (600-ns burst) along ~~semicoincident~~ semi-coincident survey trajectories in the DF region. ~~It~~ Their results implied that at the same depth modern systems would provide not only a higher resolution, but most likely also a deeper detection of continuous IRHs (Rodriguez-Morales et al., 2020). In addition, as we pointed out in Section 4.2, the EFZ visible in our radargrams is most likely caused by the radar system itself, which disables us to find the correspondence events of stagnant ice in the data.

Our sensitivity study also ~~shows~~ showed the correspondence between the age of basal ice and ice thickness, as a crucial input in the ice-flow model. Accurate ice thickness can improve the reliability of the modeling results. Our radar data ~~was~~ were collected with an incoherent burst radar system, which means hyperbolic effects in signals are strong and affect the accuracy of subglacial topography. According to ~~Tsutaki et al. (2022)~~Tsutaki et al. (2022), the average difference between ice thickness observed from ~~Japanese~~ the JARE radar system (with high-gain and high-directivity antennae) and the AWI RES system is −8 m, and the standard deviation is 108 m. The high standard deviation implies the details of the bed topography observed by two radar systems could be significantly different, which may cause the misalignment in modeling results.

Overall, the radar system we use in this study limits the number, depth and accuracy of the IRHs traced, the possibility of observing the basal unit and the resolution of bed topography observed in the radargrams, which all affect the modeling results. In contrast, despite these shortcomings the simple and light-weight system enabled a long range of the aircraft from a high-altitude field camp to cover a large region around DF. Analysis of ground-based radar observations from more sensitive radar systems with higher vertical as well as horizontal resolution in sub-regions of our larger DF area, as were already acquired in the past, will thus complement the large-scale results from our study with more accurate detailed insights.

### 4.4.2 Modelling limitations

Our model does not consider horizontal advection and assumes that the basal sliding ratio is negligible, which are proper assumptions at DF. To improve the reliability of the model results in regions further away from DF, a basal sliding term could be added. However, this would make it more difficult to infer the mechanical ice thickness, the velocity shape exponent and the sliding ratio at the same time. Furthermore, although 3-D full Stokes models can lift restrictions, they still come along with new challenges, including heavy computation time, more complicated boundary conditions and conjunction between 3-D model and age observations. For the time being, a model of intermediate complexity operating along flow lines or 2.5D approaches might provide useful results nevertheless (Gerber et al., 2023)

## 5 ~~Conclusions and perspectives~~Conclusions

We utilized a 1D ice-flow model to reconstruct the age field and analyse the basal thermal states in the DF region. The model is constrained by traced internal horizons observed in airborne radar data, which are dated by transferring ages from the DF ice-core timescales.

~~From the combination of observed internal layer stratigraphy with our 1D ice flow model We draw the following conclusions:~~

~~1. We~~ According to the modeled age of the basal ice, we identify four potential ~~candidates~~ candidate areas for old ice in the DF region: a subglacial mountainous target located around the DF drill site with a radius of $\sim$ 100 km, $\sim$ 160 km to the ~~north-west~~ west of the DF drill, $\sim$ 240 km to the ~~north-west~~ west of the DF drill and $\sim$ 260 km to the ~~south-west~~ south of DF drill. The first candidate deserves most attention since it has a good correspondence with the previous old ice predictions obtained by a very different model approach (Karlsson et al., 2018; Van Liefferinge et al., 2018). At the DF drill site, the ~~age of ice is 841.8 kaand 1034.5 ka at 100 m and 50 m above the bed, and 1345.8 ka at the ice–bed interface.~~ modeled age of the basal ice is 1347.2 ka$\pm$503.1 ka . At NDF the maximum age is extrapolated as 1472.1 ka$\pm$509.0 ka at a depth of 2080.7 m. The age of basal ice has a considerable uncertainty due to limitations in the number and depth of our IRHs, which could be mitigated by using radar data set with higher resolution, higher sensitivity and thus better traceability. Deployment of state-of-the-art radar systems might decrease this limitation and lead to improved model performance.

~~2. Modelled basal~~ The modeled basal thermal state implies that melting is more common than stagnant ice in the DF region. Modeled basal melt rates vary from 0 to ~~8.4~~8.39 mm a$^{-1}$~~, melting being~~ . Melting is significant $\sim$ 200 km ~~west~~ south–west and 150 km ~~south~~ south–east of the DF drill ~~. Stagnant ice seems to be present mainly~~ site. At the DF drill site our model produces a melt rate of 0.11$\pm$0.37 mm a$^{-1}$, which corresponds to earlier estimates. Stagnant ice is mainly present immediately north of NDF and $\sim$ 180 km ~~north-west~~ west of the DF drill ~~stie~~site. It occupies only 8 % of the radar profiles with an average thickness of 95.6 m. The region close to NDF has the most favorable conditions ~~of~~ for a cold bed ~~for~~ holding old ice. ~~There is no stagnant ice at the DF site, the melt rate at the DF drill is 0.11$\pm$0.37 mm a$^{-1}$. Compared to a~~ The thickness of stagnant ice ~~of $\sim$ 200 m in the LDC region, the basal thermal condition in the DF region is warmer.~~ is modeled as 206.5 m at NDF.

We obtain an average accumulation rate over the past 720 ka of 0.015–0.038 m a$^{-1}$ ice equivalent in the DF region and 0.022 m a$^{-1}$ ice equivalent at the DF drill site.

~~3. An~~ In our sensitive study we demonstrated that an extra IRH at deeper depth and/or using a different timescale significantly affect the model results. This underlines the importance of using IRHs traced as deep as possible and to use the most trustworthy timescale to get ~~more~~ reliable model results. ~~Regarding our results, the age of basal ice could be overestimated in the DF region because of limitations in the depth of our IRHs and because of the inability of our model to capture complex thinning phenomena in the basal layer.~~

~~Our study still has some limitations which might be considered in future approaches. Our model does not consider horizontal advection and assumes that the basal sliding ratio is negligible, which are proper assumptions at DF. To improve the reliability of model results in regions further from DF, a basal sliding term could be added, but it will be difficult to infer at the same time the mechanical ice thickness, the velocity shape exponent and the sliding ratio. Furthermore, 3-D full stokes model can lift restrictions, however, there are still challenges for 3-D models, including heavy computation time, complicated boundary~~

~~conditions and conjunction between 3-D model and age observations. Moreover, the~~ The radar system we use in the study limits the number, depth and accuracy of the IRHs traced, the possibility of observing the basal unit and the resolution of bed topography observed in the radargrams, which ~~both~~ all affect the modeling results. Using ground-based observations from improved radar systems with higher vertical as well as horizontal resolution in sub-regions of the larger DF area, as were already acquired in the past, will complement the large-scale results from our study. Our model approach is based on assumptions, like ignoring horizontal advection and basal sliding. A 3D model would partly lift these simplifications and potentially improve the reliability of model results, but would also increase the demand for computing resources and boundary conditions.

We observe an inflection point at the depth of $\sim$ 300 m above the bed in the experimental timescale of the DF ice core, which we consider to be caused by more complex flow related to basal melting. This shows the inability of our model to capture complex thinning phenomena below that depth and thus causes an overestimation of the age in the lowermost ice. Thus, we recommend to consider the modeled age of the ice shallower than 300 m above the bed (roughly 10% of the ice thickness) for decision making. At the same time, more attention should be paid to the basal thermal state, which is likely a hidden factor implying the accuracy of the modeled age. Considering the age of ice and basal thermal state together, we suggest that the area immediately north of NDF could be a potential old ice drill site in the DF region.

*Code availability.* The model code is available from Github. https://github.com/ailsachung/IsoInv1D

*Data availability.* The IRH data are available from the PANGAEA repository https://doi.org/10.1594/PANGAEA.958462 (Wang et al., 2023). The bed elevation and surface elevation data set collected by NASA Making Earth System Data Records for Use in Research Environments (MEaSUREs) program (Morlighem et al., 2017, 2020) are available on https://nsidc.org/data/nsidc-0756/versions/3. We used elevation data from the Antarctic Mapping Tools in MATLAB from https://de.mathworks.com/matlabcentral/fileexchange/47638-antarctic-mapping-tools (Greene et al., 2017). The ice thickness derived from radar data are published on https://doi.org/10.1594/PANGAEA.920234 (Eisen et al., 2020).

*Author contributions.* OE coordinated the BE–OI project and designed this study. ZW carried out experiments and wrote the manuscript with input from all co-authors. ZW and DS processed the radar data and traced the horizons. FP developed the model. AC improved and adapted the model to the conditions at Dome Fuji and performed the calculation. JF drilled the B53 ice core and provided the depth–density profile of the ice core. All coauthors read and commented on the manuscript.

*Competing interests.* O.E. is an editor of The Cryosphere. The authors declare no other competing interests.

*Acknowledgements.* This publication was generated in the frame of Beyond EPICA-Oldest Ice (BE-OI). The project has received funding from the European Union's Horizon 2020 research and innovation ~~programme~~ program under grant agreement No. 730258 (BE-OI CSA). It has received funding from the Swiss State Secretariate for Education, Research and Innovation (SERI) under contract number 16.0144. It is furthermore supported by national partners and funding agencies in Belgium, Denmark, France, Germany, Italy, Norway, Sweden, Switzerland, the Netherlands, and the United Kingdom. Logistic support is mainly provided by AWI, BAS, ENEA and IPEV. The opinions expressed and arguments employed herein do not necessarily reflect the official views of the European Union funding agency, the Swiss Government, or other national funding bodies. We thank the logistics field team and flight crew for support during the expedition. We thank Emerson E&P Software, Emerson Automation Solutions, for providing licenses in the scope of the Emerson Academic Program. We thank Brice Van Liefferinge for providing the locations of the promising old ice in the DF region in his previous study. We thank Nanna B. Karlsson, who offered the detailed locations of the subglacial lakes and the old ice candidates in her previous study. We thank Kenji Kawamura for the insightful discussions on the DFO2006+AICC2012 timescale of the Dome Fuji ice core. Zhuo Wang is funded by China Scholarship Council (No. 202106170102). Thank goes to Professor Zhaofa Zeng for supporting her in getting the grant and jointly studying abroad as her supervisor in Jilin University. Ailsa Chung is funded through the DEEPICE project, from the European Union's Horizon 2020 research and innovation ~~programme~~ program under the Marie Sklodowska-Curie grant agreement No. 955750.

## References


Ageta, Y., Azuma, Y., Fujii, Y., Fujino, K., Fujita, S., Furukawa, T., Hondoh, T., Kameda, T., Kamiyama, K., Katagiri, K., et al.: Deep ice-core drilling at Dome Fuji and glaciological studies in east Dronning Maud Land, Antarctica, Annals of Glaciology, 27, 333–337, 1998.

Beem, L. H., Young, D. A., Greenbaum, J. S., Blankenship, D. D., Cavitte, M. G., Guo, J., and Bo, S.: Aerogeophysical characterization of Titan Dome, East Antarctica, and potential as an ice core target, The Cryosphere, 15, 1719–1730, 2021.

Cavitte, M. G., Blankenship, D. D., Young, D. A., Schroeder, D. M., Parrenin, F., Lemeur, E., Macgregor, J. A., and Siegert, M. J.: Deep radiostratigraphy of the East Antarctic plateau: connecting the Dome C and Vostok ice core sites, Journal of Glaciology, 62, 323–334, 2016.

Cavitte, M. G. P.: Flow re-organization of the East Antarctic ice sheet across glacial cycles, Ph.D. thesis, 2017.

Chung, A., Parrenin, F., Steinhage, D., Mulvaney, R., Martín, C., Cavitte, M. G. P., Lilien, D. A., Helm, V., Taylor, D., Gogineni, P., Ritz, C., Frezzotti, M., O'Neill, C., Miller, H., Dahl-Jensen, D., and Eisen, O.: Stagnant ice and age modelling in the Dome C region, Antarctica, EGUsphere, 2023, 1–31, 2023.

Colgan, W., MacGregor, J. A., Mankoff, K. D., Haagenson, R., Rajaram, H., Martos, Y. M., Morlighem, M., Fahnestock, M. A., and Kjeldsen, K. K.: Topographic correction of geothermal heat flux in greenland and antarctica, Journal of Geophysical Research: Earth Surface, 126, e2020JF005 598, 2021.

Dome Fuji Ice Core Project Members, D. F. I. C. P. M.: State dependence of climatic instability over the past 720,000 years from Antarctic ice cores and climate modeling, Science advances, 3, e1600 446, 2017.

Drews, R., Eisen, O., Weikusat, I., Kipfstuhl, S., Lambrecht, A., Steinhage, D., Wilhelms, F., and Miller, H.: Layer disturbances and the radio-echo free zone in ice sheets, The Cryosphere, 3, 195–203, 2009.

Eisen, O., Steinhage, D., Karlsson, N. B., Binder, T., and Helm, V.: Ice thickness of the Oldest Ice Reconnaissance survey, 2016/17, Dome Fuji - Beyond EPICA, https://doi.org/10.1594/PANGAEA.920234, 2020.

Fischer, H., Severinghaus, J., Brook, E., Wolff, E., Albert, M., Alemany, O., Arthern, R., Bentley, C., Blankenship, D., Chappellaz, J., et al.: Where to find 1.5 million yr old ice for the IPICS" Oldest-Ice" ice core, Climate of the Past, 9, 2489–2505, 2013.

Franke, S., Gerber, T., Warren, C., Jansen, D., Eisen, O., and Dahl-Jensen, D.: Investigating the radar response of englacial debris entrained basal ice units in East Antarctica using electromagnetic forward modelling, IEEE Transactions on Geoscience and Remote Sensing, 2023.

Freitag, J., Kipfstuhl, S., and Laepple, T.: Core-scale radioscopic imaging: a new method reveals density–calcium link in Antarctic firn, Journal of Glaciology, 59, 1009–1014, 2013.

Fujita, S., Maeno, H., Uratsuka, S., Furukawa, T., Mae, S., Fujii, Y., and Watanabe, O.: Nature of radio echo layering in the Antarctic ice sheet detected by a two-frequency experiment, Journal of Geophysical Research: Solid Earth, 104, 13 013–13 024, 1999.

Fujita, S., Holmlund, P., Andersson, I., Brown, I., Enomoto, H., Fujii, Y., Fujita, K., Fukui, K., Furukawa, T., Hansson, M., et al.: Spatial and temporal variability of snow accumulation rate on the East Antarctic ice divide between Dome Fuji and EPICA DML, The Cryosphere, 5, 1057–1081, 2011.

Fujita, S., Holmlund, P., Matsuoka, K., Enomoto, H., Fukui, K., Nakazawa, F., Sugiyama, S., and Surdyk, S.: Radar diagnosis of the subglacial conditions in Dronning Maud Land, East Antarctica, The Cryosphere, 6, 1203–1219, 2012.

Fujita, S., Parrenin, F., Severi, M., Motoyama, H., and Wolff, E.: Volcanic synchronization of Dome Fuji and Dome C Antarctic deep ice cores over the past 216 kyr, Climate of the Past, 11, 1395–1416, 2015.

Gerber, T. A., Lilien, D. A., Rathmann, N. M., Franke, S., Young, T. J., Valero-Delgado, F., Ershadi, M. R., Drews, R., Zeising, O., Humbert, A., et al.: Crystal orientation fabric anisotropy causes directional hardening of the Northeast Greenland Ice Stream, Nature Communications, 14, 2653, 2023.

Greene, C. A., Gwyther, D. E., and Blankenship, D. D.: Antarctic mapping tools for MATLAB, Computers & Geosciences, 104, 151–157, 2017.

Hondoh, T., Shoji, H., Watanabe, O., Salamatin, A. N., and Lipenkov, V. Y.: Depth–age and temperature prediction at Dome Fuji station, East Antarctica, Annals of Glaciology, 35, 384–390, 2002.

Jouzel, J. and Masson-Delmotte, V.: Deep ice cores: the need for going back in time, Quaternary Science Reviews, 29, 3683–3689, 2010.

Kameda, T., Fujita, K., Sugita, O., Hirasawa, N., and Takahashi, S.: Total solar eclipse over Antarctica on 23 November 2003 and its effects on the atmosphere and snow near the ice sheet surface at Dome Fuji, Journal of Geophysical Research: Atmospheres, 114, 2009.

Karlsson, N. B., Binder, T., Eagles, G., Helm, V., Pattyn, F., Van Liefferinge, B., and Eisen, O.: Glaciological characteristics in the Dome Fuji region and new assessment for "Oldest Ice", The Cryosphere, 12, 2413–2424, 2018.

Karlsson, N. B., Binder, T., Eagles, G., Helm, V., Pattyn, F., Van Liefferinge, B., and Eisen, O.: Ice thickness from the Dome Fuji region, East Antarctica from ice-penetrating radar, https://doi.org/10.1594/PANGAEA.891323, 2018.

Kawamura, K., Parrenin, F., Lisiecki, L., Uemura, R., Vimeux, F., Severinghaus, J. P., Hutterli, M. A., Nakazawa, T., Aoki, S., Jouzel, J., et al.: Northern Hemisphere forcing of climatic cycles in Antarctica over the past 360,000 years, Nature, 448, 912–916, 2007.

Lilien, D. A., Steinhage, D., Taylor, D., Parrenin, F., Ritz, C., Mulvaney, R., Martín, C., Yan, J.-B., O'Neill, C., Frezzotti, M., Miller, H., Gogineni, P., Dahl-Jensen, D., and Eisen, O.: Brief communication: New radar constraints support presence of ice older than 1.5 Myr at Little Dome C, The Cryosphere, 15, 1881–1888, 2021.

Lisiecki, L. E. and Raymo, M. E.: A Pliocene-Pleistocene stack of 57 globally distributed benthic $\delta^{18}$O records, Paleoceanography, 20, 2005.

Lliboutry, L.: A critical review of analytical approximate solutions for steady state velocities and temperatures in cold ice-sheets, Z. Gletscherkde. Glazialgeol., 15, 135–148, 1979.

Morlighem, M.: MEaSUREs BedMachine Antarctica, Version 3 [Data Set], https://doi.org/10.5067/FPSU0V1MWUB6, date Accessed 05-30-2022, 2022.

Morlighem, M., Williams, C. N., Rignot, E., An, L., Arndt, J. E., Bamber, J. L., Catania, G., Chauché, N., Dowdeswell, J. A., Dorschel, B., et al.: BedMachine v3: Complete bed topography and ocean bathymetry mapping of Greenland from multibeam echo sounding combined with mass conservation, Geophysical research letters, 44, 11–051, 2017.

Morlighem, M., Rignot, E., Binder, T., Blankenship, D., Drews, R., Eagles, G., Eisen, O., Ferraccioli, F., Forsberg, R., Fretwell, P., et al.: Deep glacial troughs and stabilizing ridges unveiled beneath the margins of the Antarctic ice sheet, Nature Geoscience, 13, 132–137, 2020.

Motoyama, H.: The second deep ice coring project at Dome Fuji, Antarctica, Scientific Drilling, 5, 41–43, 2007.

Motoyama, H., Takahashi, A., Tanaka, Y., Shinbori, K., Miyahara, M., Yoshimoto, T., Fujii, Y., Furusaki, A., Azuma, N., Ozawa, Y., et al.: Deep ice core drilling to a depth of 3035.22 m at Dome Fuji, Antarctica in 2001–07, Annals of Glaciology, 62, 212–222, 2021.

Mouginot, J., Scheuchl, B., and Rignot, E.: Mapping of ice motion in Antarctica using synthetic-aperture radar data, Remote Sensing, 4, 2753–2767, 2012.

Mouginot, J., Rignot, E., Scheuchl, B., and Millan, R.: Comprehensive annual ice sheet velocity mapping using Landsat-8, Sentinel-1, and RADARSAT-2 data, Remote Sensing, 9, 364, 2017.

Nixdorf, U., Steinhage, D., Meyer, U., Hempel, L., Jenett, M., Wachs, P., and Miller, H.: The newly developed airborne radio-echo sounding system of the AWI as a glaciological tool, Annals of Glaciology, 29, 231–238, 1999.

Obase, T., Abe-Ouchi, A., Saito, F., Tsutaki, S., Fujita, S., Kawamura, K., and Motoyama, H.: A one-dimensional temperature and age modeling study for selecting the drill site of the oldest ice core near Dome Fuji, Antarctica, The Cryosphere, 17, 2543–2562, https://doi.org/10.5194/tc-17-2543-2023, 2023.

Parrenin, F., Hindmarsh, R., and Rémy, F.: Analytical solutions for the effect of topography, accumulation rate and lateral flow divergence on isochrone layer geometry, Journal of Glaciology, 52, 191–202, 2006.

Parrenin, F., Dreyfus, G., Durand, G., Fujita, S., Gagliardini, O., Gillet, F., Jouzel, J., Kawamura, K., Lhomme, N., Masson-Delmotte, V., et al.: 1-D-ice flow modelling at EPICA Dome C and Dome Fuji, East Antarctica, Climate of the Past, 3, 243–259, 2007.

Parrenin, F., Cavitte, M. G., Blankenship, D. D., Chappellaz, J., Fischer, H., Gagliardini, O., Masson-Delmotte, V., Passalacqua, O., Ritz, C., Roberts, J., et al.: Is there 1.5-million-year-old ice near Dome C, Antarctica?, The Cryosphere, 11, 2427–2437, 2017.

Raisbeck, G., Yiou, F., Cattani, O., and Jouzel, J.: 10Be evidence for the Matuyama–Brunhes geomagnetic reversal in the EPICA Dome C ice core, Nature, 444, 82–84, 2006.

Raymo, M. E., Lisiecki, L., and Nisancioglu, K. H.: Plio-Pleistocene ice volume, Antarctic climate, and the global $\delta$18O record, Science, 313, 492–495, 2006.

Rignot, E., Mouginot, J., and Scheuchl, B.: Ice flow of the Antarctic ice sheet, Science, 333, 1427–1430, 2011.

Rignot, E., Mouginot, J., and Scheuchl, B.: MEaSUREs InSAR-Based Antarctica Ice Velocity Map, Version 2, https://doi.org/10.5067/D7GK8F5J8M8R, 2017.

Rodriguez-Morales, F., Braaten, D., Mai, H. T., Paden, J., Gogineni, P., Yan, J.-B., Abe-Ouchi, A., Fujita, S., Kawamura, K., Tsutaki, S., et al.: A Mobile, Multichannel, UWB Radar for Potential Ice Core Drill Site Identification in East Antarctica: Development and First Results, IEEE Journal of Selected Topics in Applied Earth Observations and Remote Sensing, 13, 4836–4847, 2020.

Saruya, T., Fujita, S., Iizuka, Y., Miyamoto, A., Ohno, H., Hori, A., Shigeyama, W., Hirabayashi, M., and Goto-Azuma, K.: Development of crystal orientation fabric in the Dome Fuji ice core in East Antarctica: implications for the deformation regime in ice sheets, The Cryosphere, 16, 2985–3003, 2022.

Seddik, H., Greve, R., Zwinger, T., and Placidi, L.: A full Stokes ice flow model for the vicinity of Dome Fuji, Antarctica, with induced anisotropy and fabric evolution, The Cryosphere, 5, 495–508, 2011.

Singer, B. and Brown, L. L.: The Santa Rosa Event: 40Ar/39Ar and paleomagnetic results from the Valles rhyolite near Jaramillo Creek, Jemez Mountains, New Mexico, Earth and Planetary Science Letters, 197, 51–64, 2002.

Sun, B., Moore, J. C., Zwinger, T., Zhao, L., Steinhage, D., Tang, X., Zhang, D., Cui, X., and Martín, C.: How old is the ice beneath Dome A, Antarctica?, The Cryosphere, 8, 1121–1128, 2014.

Sutter, J., Fischer, H., and Eisen, O.: Investigating the internal structure of the Antarctic ice sheet: the utility of isochrones for spatiotemporal ice-sheet model calibration, The Cryosphere, 15, 3839–3860, 2021.

Talalay, P., Li, Y., Augustin, L., Clow, G. D., Hong, J., Lefebvre, E., Markov, A., Motoyama, H., and Ritz, C.: Geothermal heat flux from measured temperature profiles in deep ice boreholes in Antarctica, The Cryosphere, 14, 4021–4037, 2020.

Tsutaki, S., Fujita, S., Kawamura, K., Abe-Ouchi, A., Fukui, K., Motoyama, H., Hoshina, Y., Nakazawa, F., Obase, T., Ohno, H., Oyabu, I., Saito, F., Sugiura, K., and Suzuki, T.: High-resolution subglacial topography around Dome Fuji, Antarctica, based on ground-based radar surveys over 30 years, The Cryosphere, 16, 2967–2983, 2022.

Van Liefferinge, B. and Pattyn, F.: Using ice-flow models to evaluate potential sites of million year-old ice in Antarctica, Climate of the Past, 9, 2335–2345, 2013.

Van Liefferinge, B., Pattyn, F., Cavitte, M. G., Karlsson, N. B., Young, D. A., Sutter, J., and Eisen, O.: Promising Oldest Ice sites in East Antarctica based on thermodynamical modelling, The Cryosphere, 12, 2773–2787, 2018.

Wang, Z., Chung, A., Steinhage, D., Parrenin, F., Freitag, J., and Eisen, O.: Radar internal layer stratigraphy in the Dome Fuji region, Antarctica, https://doi.org/10.1594/PANGAEA.958462, 2023.

Watanabe, O., Kamiyama, K., Motoyama, H., Fujii, Y., Shoji, H., and Satow, K.: The paleoclimate record in the ice core at Dome Fuji station, East Antarctica, Annals of Glaciology, 29, 176–178, 1999.

Wesche, C., Steinhage, D., and Nixdorf, U.: Polar aircraft Polar5 and Polar6 operated by the Alfred Wegener Institute, Journal of large-scale research facilities, 2, 1–7, 2016.

Willeit, M., Ganopolski, A., Calov, R., and Brovkin, V.: Mid-Pleistocene transition in glacial cycles explained by declining CO2 and regolith removal, Science Advances, 5, eaav7337, 2019.

Winter, A., Steinhage, D., Arnold, E. J., Blankenship, D. D., Cavitte, M. G., Corr, H. F., Paden, J. D., Urbini, S., Young, D. A., and Eisen, O.: Comparison of measurements from different radio-echo sounding systems and synchronization with the ice core at Dome C, Antarctica, The Cryosphere, 11, 653–668, 2017.

Young, D. A., Roberts, J. L., Ritz, C., Frezzotti, M., Quartini, E., Cavitte, M. G., Tozer, C. R., Steinhage, D., Urbini, S., Corr, H. F., et al.: High-resolution boundary conditions of an old ice target near Dome C, Antarctica, The Cryosphere, 11, 1897–1911, 2017.

**Supplementary Material**

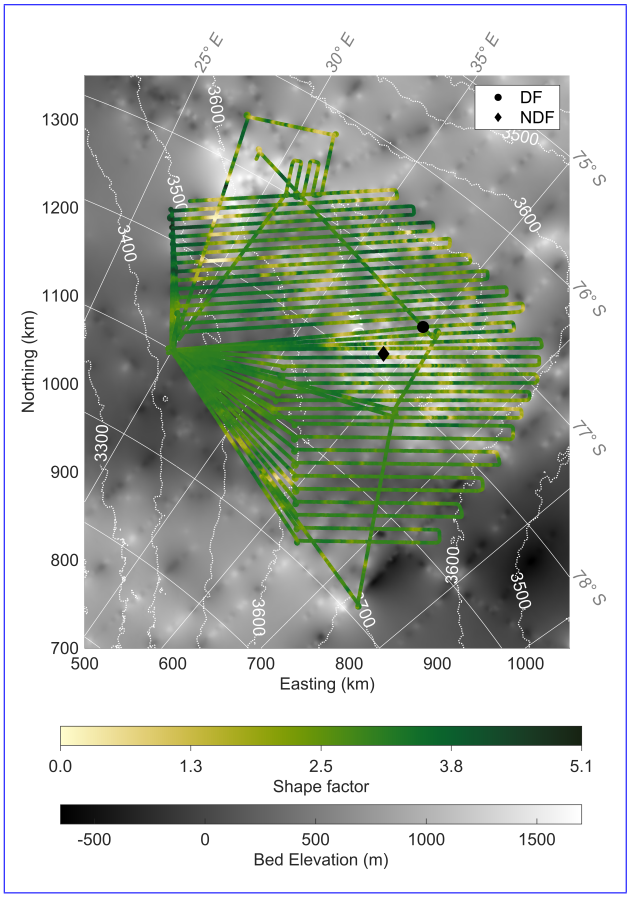


**Figure S1.** Shape factor along the profiles of the radar survey in the DF region. The interpolated shape ~~factor~~ factors at the DF drill site and the NDF are ~~interpolated as~~ 3.1 and 2.2, respectively.

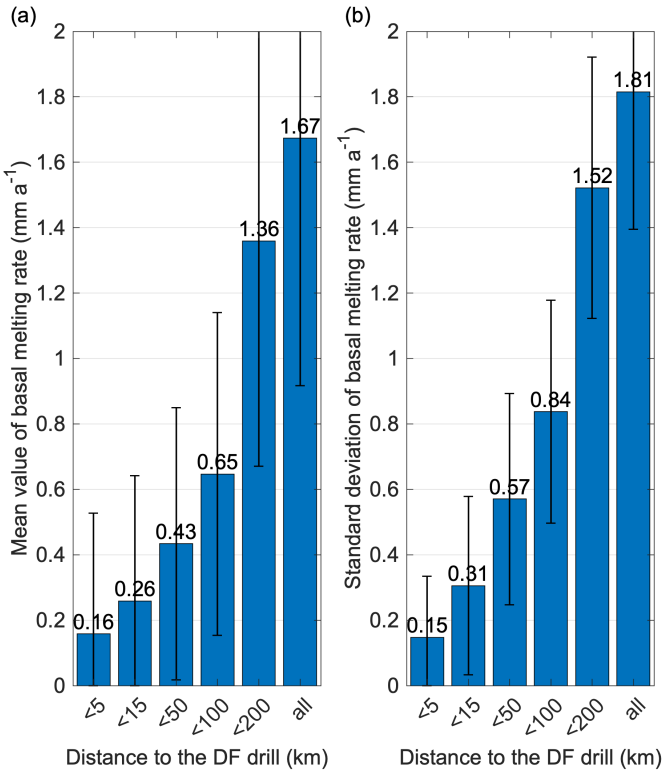


**Figure S2.** (a) Spatial mean value and (b) spatial standard deviation of deduced basal melt rates within 5, 15, 50, 200 km to the DF drill site. Error bars show the corresponding mean value and spatial standard deviation of uncertainties of basal melt rates, which are output together with melt rates from the model. The last bar "all" represents the whole study area. Numbers on the bars indicate the actual values.

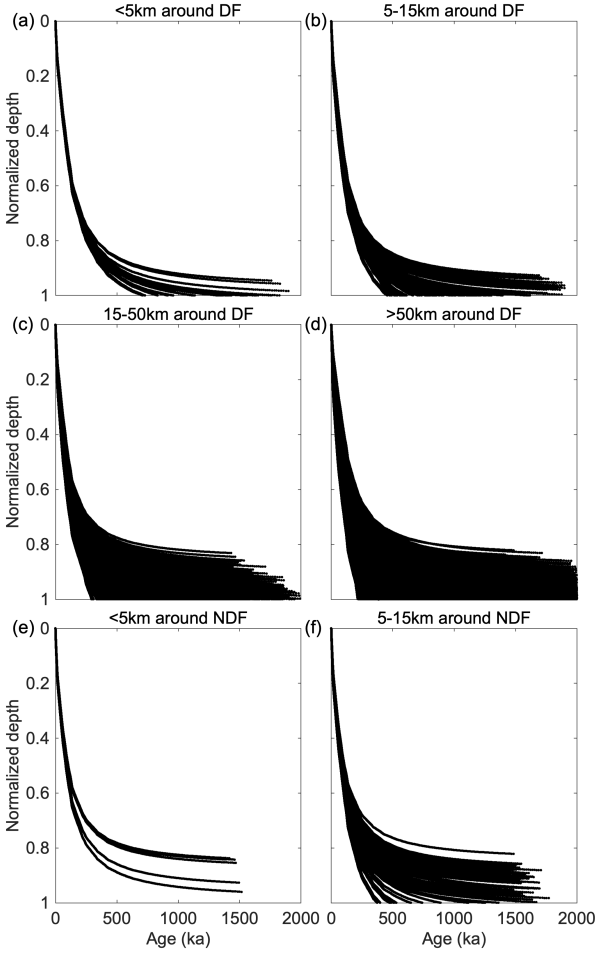


**Figure S3.** Vertically ~~normalized~~ depth-normalized (0 at surface and 1 at ice-bed interface) age–depth ~~distribution~~ distributions in distance ranges (a) < 5, (b) 5–15, (c) 15–50, (d) > 50 km around DF and (e) < 5, (f) 5–15 km around NDF. The distributions in ranges 15–50 km and > 50 km around NDF have similar shapes to those around DF. ~~It shows the relation between age and normalized depth (0 on surface and 1 at ice-bed interface) in different areas around DF and NDF, respectively.~~ By normalization we remove ~~in principle~~ the effect of varying ice thickness, as internal ~~layers~~ horizons (and thus age) ~~follows~~ follow the bed topography to a first degree. The normalized age–depth distributions 5 km and 5–15 km around DF and NDF show less spreading in age compared with those farther away.

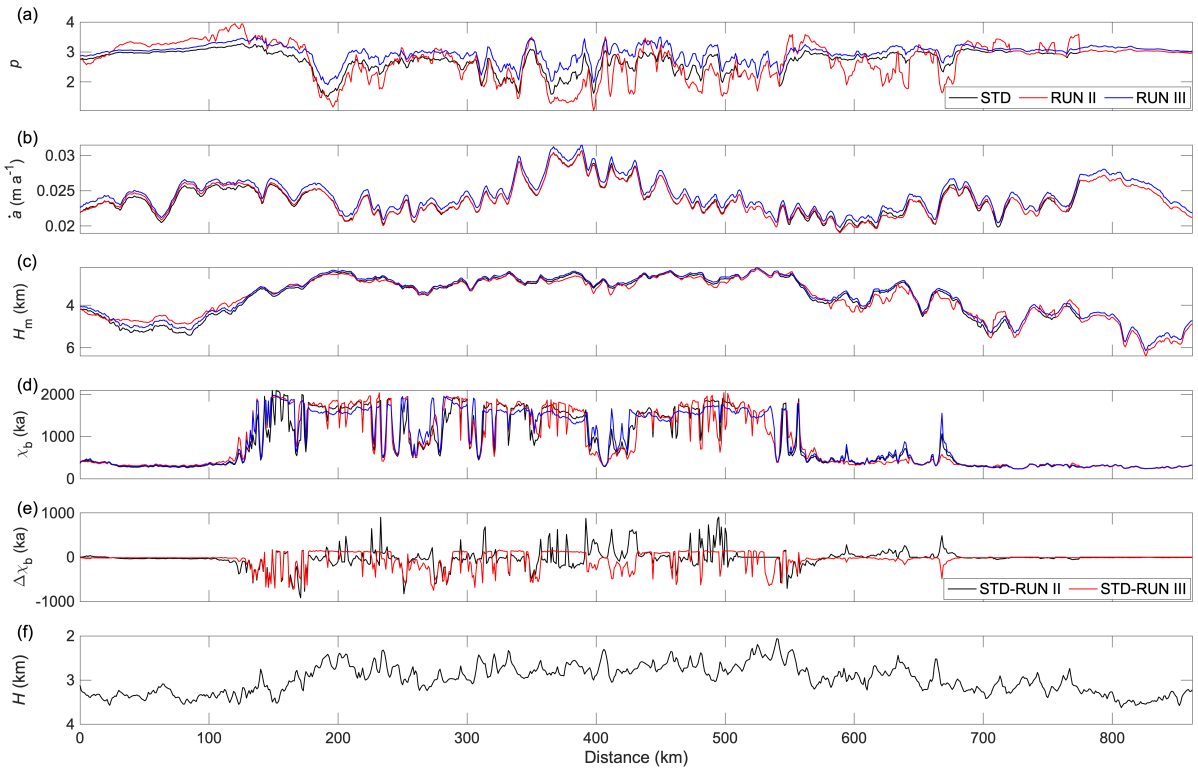


**Figure S4.** Comparison of (a) shape factor $p$, (b) accumulation rate $\dot{a}$, (c) mechanical ice thickness $H_m$, (d) age of basal ice $\chi_b$ ~~between~~ for three runs ~~,~~ (black line: STD, red line~~and~~ : RUN II, blue line~~show the modeling result of runs STD, II and~~ : RUN III~~, respectively~~). (e) The difference of age of basal ice $\delta\chi_b$ between STD and RUN II (~~in~~ black~~line~~), and between STD and RUN III (~~in~~ red~~line~~). (f) Ice thickness $H$ observed ~~from~~ with radar ~~system~~ (Karlsson et al., 2018). An overlap between STD and RUN II implies that there is no additional information of the EH8 in those areas (514–543 km, 644–650 km, 705–708 km, 722–744 km, 757–765 km and 776–863 km), which means the results of the two runs are ~~totally the same there~~ similar and return same results. We find that difference of the shape factor (Fig. S4a) between STD and RUN II are relatively significant along the profile, especially at the distance from $\sim$ 0 km to $\sim$ 120 km, and from $\sim$ 590 km to $\sim$ 780 km (~~exclude~~ excluding the overlap areas). While STD and RUN III basically keep a similar difference in the whole profile~~and~~ , the shape factor of STD stays smaller than in RUN III. The difference of accumulation rates between STD and RUN III has a similar value of $\sim$ 0.0007 at each point along the profile, while the difference between STD and RUN II is negligible (Fig. S4b). The difference of mechanical ice thickness between STD and RUN II/RUN III are larger from 0 to 110 km, and from 580 to 710 km. In other places, the difference is tiny (Fig. S4c). From 580 to 700 km, we can observe a more ~~turbulent~~ spatially varying difference between STD and RUN II than RUN III. The age of basal ice at different points along the profile has a notable difference (Fig. S4d). For clarity we show the difference additionally between each two model runs in Fig. S4e. Occasional peaks of ~~STD-RUN~~ STD minus RUN III, e.g. at distance of $\sim$ 150 km, $\sim$ 170 km and $\sim$ 530 km, reach a difference of up to $\sim$ 800 ka. The differences between STD and RUN II is larger, up to $\sim$ 920 ka at $\sim$ 250 km, where EH8 was not traced the difference is 0. We find that the peaks ~~of~~ in difference between STD and RUN II and III ~~/RUN~~ can be often observed at the same places, e.g. $\sim$ 150 km, $\sim$ 250 km, $\sim$ 490 km, together with peaks of bed topography (Fig. S4f), which implies that the topography is a important factor for age.

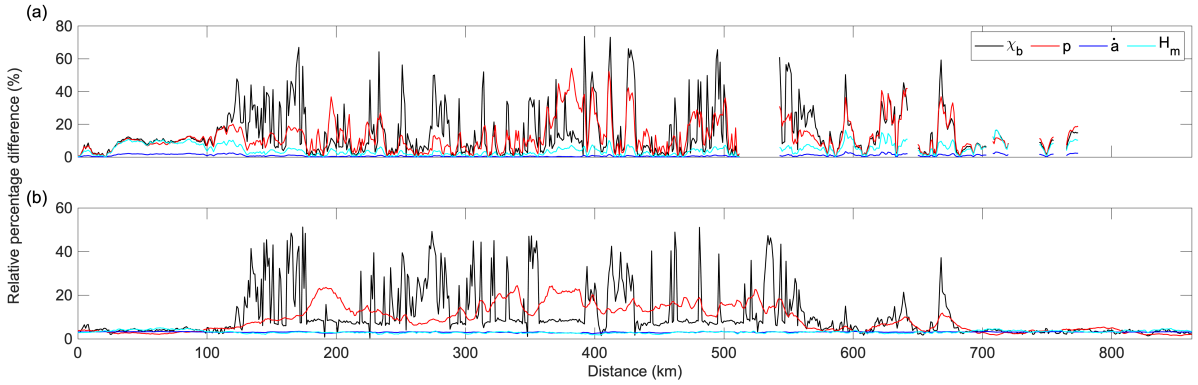


**Figure S5.** Relative percentage difference of the accumulation rate $\dot{a}$, the shape factor $p$, the mechanical ice thickness $H_m$ and the age of basal ice $\chi_b$ ~~between~~ derived from (a) STD ~~and~~ minus RUN II, (b) STD ~~and~~ minus RUN III. We find that at many points the relative percentage difference of the shape factor and the age of the basal ice fluctuate simultaneously, e.g., from 0 to 100 km in Fig. S5a. ~~But this synchrony doesn't~~ However, such a synchronous behaviour does not always ~~happens~~prevail, e.g. from 140 km to 150 km in Fig. S5a, and from 350 km to 400 km in Fig. S5b. The fluctuations of relative percentage difference of the accumulation rate in both scenarios are tiny along the profile. The relative percentage difference of mechanical ice thickness between STD ~~and~~ minus RUN II basically follow the change of relative percentage difference of the shape factor, but with a much lower value.

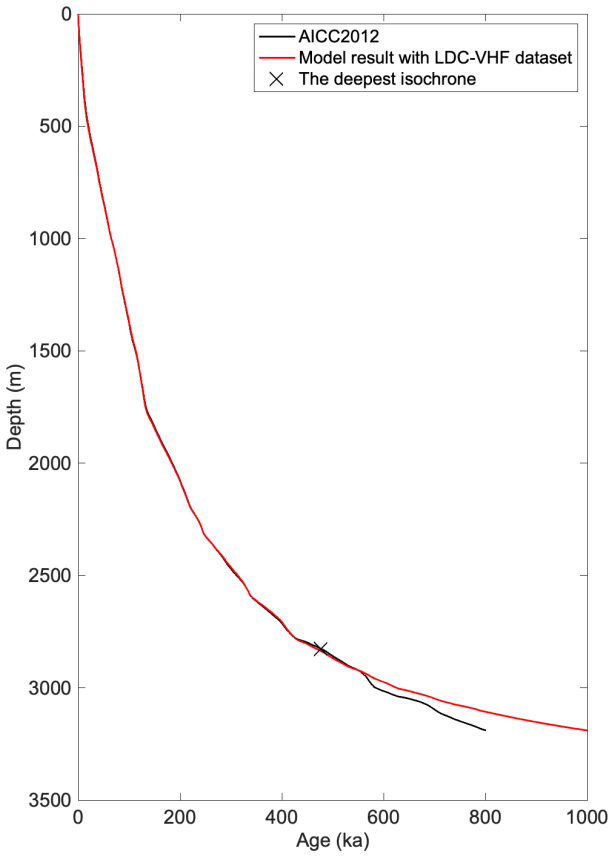


**Figure S6.** Model derived age–depth scale and AICC2012 timescale at EDC. (Chung et al., 2023)